Materials & Design 263 (2026) 115650

Contents lists available at ScienceDirect

Materials & Design

journal homepage: www.elsevier.com/locate/matdes

Metal surface passivation in semiconductor processing of Mo, W, TiN/TiSiN, and Cu: emerging strategies for corrosion and etching control

Yejin Lee [a,1], Suyeon Bae [a,1], Jee Woo Kim [a,1], Byungjoon Kang [b], Sungmin Kim [b], Jina Kim [b], Insun Park [b], Kyu Young Hwang [b], Byung-Kwon Kim [a,c,*]

[a] Department of Chemistry and Nanoscience, Ewha Womans University, Seoul 03760, Republic of Korea
[b] Samsung Advanced Institute of Technology, Samsung Electronics Co. Ltd., Suwon-si, Gyeonggi-do 16678, Republic of Korea
[c] Institute for Multiscale Matter and Systems (IMMS), Ewha Womans University, Seoul 03760, Republic of Korea

ARTICLE INFO

Keywords:
Atomic layer deposition
Chemical mechanical polishing
Corrosion control
Corrosion inhibitors
Semiconductor processing
Surface passivation

ABSTRACT

Wet cleaning, a critical step in semiconductor manufacturing, is essential for device reliability but can induce metal corrosion due to the aggressive chemical solutions used, becoming a primary cause of yield degradation. As device miniaturization and the complexity of 3D structures advance, the use of nanometer-scale metal thin films and dissimilar metal junctions has become commonplace, further increasing the importance of corrosion control. This review systematically examines the corrosion mechanisms and state-of-the-art passivation strategies for key metallic materials—molybdenum (Mo), titanium-based nitrides, tungsten (W), and copper (Cu)—that critically influence the performance and reliability of next-generation semiconductor devices. For each metal, a wide range of corrosion control technologies are discussed, from chemical inhibitors based on organic compounds and amino acids to advanced techniques such as graphene and ceramic nanocoating, film quality control using Chemical Vapor Deposition (CVD) and Atomic Layer Deposition (ALD), interface engineering strategies like hydrothermal oxidation (HTO), self-passivation, and innovative strategies like self-healing and metal–organic framework (MOF)-based hybrid coatings. This paper demonstrates that a multifaceted approach combining chemical inhibition with the formation of physical protective barriers is a key strategy for ensuring the interfacial stability of metals and enhancing device reliability in next-generation semiconductor processes.

1. Introduction

The performance and reliability of modern semiconductor devices are fundamentally determined by precisely controlled fabrication processes, among which wet cleaning—aimed at removing contaminants from the wafer surface and maintaining chemical uniformity—is one of the most critical and frequently performed steps [1–3]. Wet cleaning is repeatedly applied at various stages of device fabrication, including pre- and post-lithography, after deposition and etching, following ion implantation, and post-chemical mechanical polishing (CMP). Owing to its

Abbreviations: AA, Alcohol amine; AFM, Atomic force microscopy; AIA, Indazole-5-amine; ALD, Atomic layer deposition; AS-ALD, Area-selective atomic layer deposition; ATA, 3-Amino-1,2,4-triazole; ATAH, 5-Aminotetrazole; a-C, Amorphous carbon; BTA, Benzotriazole; BTA-MOF, Benzotriazole–metal–organic framework; BTC, Benzethonium chloride; CMP, Chemical mechanical polishing; CMPa, Chemical mechanical planarization; CPD, Cataphoretic deposition; CVD, Chemical vapor deposition; DA, Decanoic acid; DFT, Density functional theory; DCMS, Direct current magnetron sputtering; EDS, Energy dispersive spectroscopy; EIS, Electrochemical impedance spectroscopy; E_{corr}, Electrochemical corrosion potential; FA, Fulvic acid; GC, Guanidine carbonate; HEDP, Hydroxyethylidene diphosphonic acid; HiPIMS, High power impulse magnetron sputtering; HTO, Hydrothermal oxidation; i_{corr}, Corrosion current density; k, Dielectric constant; $K_4P_2O_7$, Potassium pyrophosphate; MAIP, Multi-arc ion plating; MOF, Metal–organic framework; MRR, Material removal rate; MTAH, 5-mercapto-1-methyltetrazole; MTEZ, 5-methyltetrazole; N,S-CDs, Nitrogen, sulfur-co doped carbon dots; OCP, Open circuit potential; PDP, Potentiodynamic polarization; PEALD, Plasma-enhanced atomic layer deposition; PR, Photoresist; RR, Removal rate; R_p, Polarization resistance; SAM, Self-assembled monolayer; SC-1, Standard clean 1; SC-2, Standard clean 2; SEM, Scanning electron microscopy; SER, Static etching rate; SHA, Salicylhydroxamic acid; STEM, Scanning Transmission Electron Microscopy; STR, Small triazole derivative; TAZ, 1,2,4-triazole; TDMAT, Tetrakisdimethylaminotitanium; TEM, Transmission electron microscopy; TEZ, Tetrazole; TMAH, Tetramethylammonium hydroxide; TTA, Tolyltriazole; XPS, X-ray photoelectron spectroscopy.

* Corresponding author at: Department of Chemistry and Nanoscience, Ewha Womans University, Seoul 03760, the Republic of Korea.
E-mail address: kimb@ewha.ac.kr (B.-K. Kim).

[1] These authors contributed equally to this work.

https://doi.org/10.1016/j.matdes.2026.115650
Received 28 October 2025; Received in revised form 9 February 2026; Accepted 10 February 2026
Available online 14 February 2026

repeated application and direct interaction with exposed materials, the effectiveness of wet cleaning is closely linked to overall process stability and device yield (Fig. 1).

To eliminate organic residues, metallic contaminants, and particulate defects, semiconductor manufacturing relies on highly oxidative or strongly acidic/alkaline chemistries such as Standard clean 1 (SC-1), Standard clean 2 (SC-2), dilute hydrofluoric acid (HF), and piranha solutions [4–6]. While these formulations ensure high cleaning efficiency, they also create chemically aggressive environments that destabilize exposed metal surfaces. Elevated temperatures, high oxidant concentrations, and extreme pH conditions further intensify interfacial reactions, increasing the susceptibility of thin metallic films to corrosion.

As device dimensions continue to scale and integration density increases, metallic films with thicknesses of only a few nanometers are routinely employed, often in close proximity to dissimilar materials. Under such conditions, electrochemical interactions—including galvanic coupling between adjacent metal layers—can give rise to highly localized corrosion phenomena that are difficult to suppress through intrinsic passivation alone [7–10]. These effects are particularly pronounced in complex multilayer stacks and high-aspect-ratio device architectures, where localized material degradation can compromise structural integrity and electrical performance (Table 1).

This challenge is critical for key metals and metal nitrides—including molybdenum (Mo), titanium-based nitrides, tungsten (W), and copper (Cu)—which serve as gate electrodes, contacts, and diffusion barriers and are repeatedly exposed to aggressive cleaning environments [11–16]. Each material exhibits distinct corrosion pathways governed by its intrinsic physicochemical properties. For example, Mo readily forms chemically unstable oxides susceptible to dissolution, titanium-based nitrides suffer from localized degradation following surface oxidation, W undergoes rapid oxidative attack in corrosive solutions, and Cu remains prone to corrosion and galvanic interactions during CMP and wet cleaning despite its favorable electrical properties [17–26].

Given that wet cleaning is inseparable from advanced semiconductor processing, ensuring the chemical and electrochemical stability of these metals is as critical as achieving effective contaminant removal. Accordingly, a comprehensive understanding of corrosion mechanisms and the development of robust, process-compatible passivation strategies are essential for sustaining device reliability as scaling and integration complexity progress.

Therefore, this review systematically examines the fundamental corrosion behaviors of Mo, titanium-based nitrides, W, and Cu under semiconductor wet cleaning conditions, and critically surveys state-of-the-art passivation and inhibition strategies developed to mitigate these challenges. By integrating mechanistic insights with materials- and process-level considerations, this work aims to provide a coherent framework for corrosion control in next-generation semiconductor manufacturing.

2. Fundamentals of metal corrosion in semiconductor wet cleaning

In semiconductor manufacturing, wet cleaning is a repeatedly applied unit process for removing organic residues, metallic contaminants, particulates, and process byproducts from wafer surfaces [27,28]. It is used at multiple fabrication stages, including photolithography, etching, ion implantation, and CMP. In practice, wet cleaning can account for more than 30% of the total fabrication flow, leading to frequent exposure of thin metallic films to strongly acidic, alkaline, or oxidizing environments, often at elevated temperatures. As device dimensions scale to the nanometer regime, even minor disruption of native or process-induced passivation layers can initiate electrochemical dissolution. Repeated exposure to aggressive chemistries amplifies this effect, causing cumulative thinning, interfacial degradation, and increased electrical resistance, even in the absence of visible defects. Accordingly, corrosion during wet cleaning should be regarded as a process-integrated electrochemical phenomenon that governs the stability of nanoscale metal features [29,30].

2.1. Overview of wet cleaning processes in semiconductor manufacturing

Wet cleaning is an essential step in semiconductor fabrication, and different formulations are applied depending on the process sequence, with SC-1, SC-2, HF, and piranha solution being the most widely used [31]. SC-1 (e.g., $NH_4OH/H_2O_2/H_2O$) is primarily employed to remove organic residues and fine particulates, where NH_4OH promotes particle dispersion and metal complexation, while H_2O_2 oxidizes carbonaceous contaminants [32,33]. SC-2 (e.g., $HCl/H_2O_2/H_2O$) targets residual metallic impurities such as Fe^{3+} and Al^{3+} through oxidative dissolution and chloride complexation, suppressing metal redeposition after SC-1 treatment [34]. Dilute HF selectively removes native SiO_2 and transition-metal oxides via fluorocomplex formation and is commonly used in pre-diffusion cleaning, gate oxide preparation, and post-etch residue removal [35]. Piranha solution (e.g., H_2SO_4/H_2O_2) is a strong oxidizing mixture that decomposes organic contaminants through the generation of reactive oxygen species, enabling efficient removal of photoresist residues and hydrocarbon films [36,37].

The effectiveness of wet cleaning is governed by oxidizing strength, metal-ion complexation, particle removal mechanisms, and compatibility with device materials [27]. These factors define the chemical environments experienced by exposed metal layers and establish the boundary conditions for corrosion phenomena [38–41].

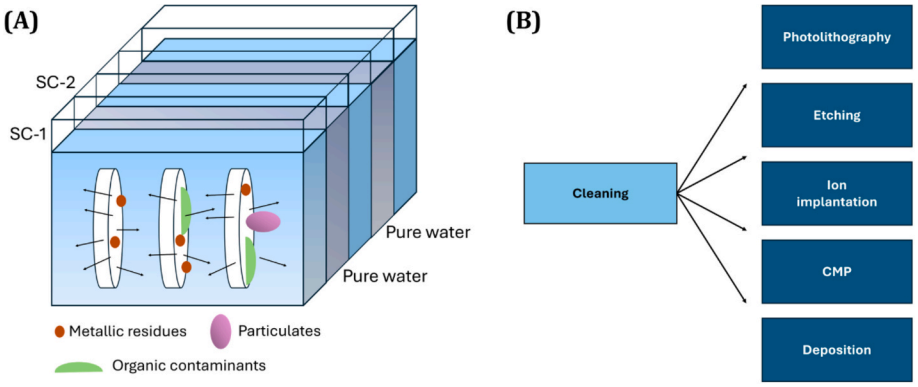

Fig. 1. (A) Schematic representation of wafer wet cleaning using sequential solutions (e.g., SC-1, SC-2) and pure water rinsing to remove organic residues, metallic ions, and particulates. (B) Illustration of wet cleaning as an integrated process step in semiconductor manufacturing, applied before and after key stages such as photolithography, etching, ion implantation, CMP, and deposition.

Table 1
Summary of corrosion inhibition effects of various inhibitors on Mo surfaces.

Inhibitor/ Coating Type	Conditions	Key Observations/ Results	Corrosion Inhibition Efficiency
BTA	0.9 wt% H_2O_2 + 0.1 wt % $K_4P_2O_7$, pH 10.0, with 0–500 ppm BTA.	Reduces Mo etch rate to 136 Å/min; E_{corr} shift + 129 mV; less dense film than ATA.	< 35.2% [74]
ATA	0.9 wt% H_2O_2 + 0.1 wt % $K_4P_2O_7$, pH 10.0, with 0–500 ppm ATA.	Etch rate: 36 Å/min; E_{corr} shift + 154 mV; dense passivation film formation.	< 89% [74]
BTA + $K_4P_2O_7$ mixture	0.1 wt% $K_4P_2O_7$ + 0.9 wt% H_2O_2, pH 10, with 200 ppm BTA.	Mo RR: 308 Å/min; ΔE: 3 mV; Mo°: 2.4% to MoO_3: 33.6%.	< 85.9% [75]
Methionine	1 wt% SiO_2 + 1 wt% H_2O_2, pH 2, with 10 mM amino acid additives.	Electron-donating groups stabilize MoO_2 surface; Mo etch rate: 26 Å/min.	< 38.9% [80]
Glycine	Slurries containing H_2O_2 and glycine at various concentrations, pH adjusted to 9–10 using KOH and $NaNO_3$.	At low conc., electrostatic interaction with Mo surface delays MoO_3 formation; at high conc., surface chelate formation can destabilize Mo and promote dissolution. Inhibition effect also confirmed in alkaline H_2O_2-based slurry systems.	< 35% [80,82]
Streptomycin	3.0 M H_3PO_4 + 1.0 M NaCl, with 10 mM streptomycin.	Suppressed Mo corrosion and H_2 evolution; protective layer confirmed by SEM.	< 98.85% [83]
Graphene coating	Graphene-coated Mo (Gr/Mo) in 0.1 M NaCl under OCP for 10 days.	Defect-minimized mono-/bilayer graphene; improved initial corrosion resistance.	< 20.8% [93]
ZrO_2 glassy coating	ZrO_2-containing glass (5–30 wt%) coated Mo were heated at 1000 °C for 2 h and annealed at 520 °C for 30 min.	Uniform bilayer graphene; reduced surface oxides.	< 75% [96]
$MoSi_2$-ZrB_2 composite coating	Mo/Zr-B4C-coated TZM alloy in 1600 °C static air.	Formation of viscous protective layer; 5-fold enhancement in Mo oxidation resistance.	Not specified [97]
Al_2O_3 / Cr_2O_3 doped Mo alloys	Mo–Al_2O_3–Cr_2O_3-coated Mo alloy after 1850–1550 °C vacuum sintering and 1200 °C vacuum annealing.	Multilayer structure; $ZrSiO_4$-containing oxide scale blocks oxygen diffusion.	Not specified [98]
TiC/ZrC carbide phases with carbon coating	Mo-C@ZrC-C@TiC-coated Mo alloy after 1950 °C sintering and rolling.	Inhibited grain growth; mechanical strength up to 862 MPa.	Not specified [99]

*Note: The corrosion inhibition efficiencies reported in this table are derived under varying experimental conditions (e.g., pH, temperature, and oxidant concentration) and are not directly comparable across different studies.

2.2. Corrosion mechanisms in wet cleaning

Metal corrosion in semiconductor wet cleaning environments is governed primarily by electrochemical dissolution under strongly oxidizing conditions. Oxidants (e.g., H_2O_2), in combination with acidic (e.g., HCl) or alkaline (e.g., NH_4OH) media, impose high solution potentials and enhance ionic transport. Upon exposure, anodic dissolution initiates at defects in oxide films, while cathodic reduction of oxidants sustains the reaction. Consequently, corrosion during wet cleaning is governed by a combination of redox kinetics and chemical etching, and oxide stability reflects a dynamic balance between oxide formation and oxidant-assisted dissolution under nonequilibrium processing conditions. Under these conditions, anodic oxidation typically produces surface oxides or hydroxides that are only transiently stable, as illustrated by representative reactions (Table 2).

- **Mo:** $Mo(s) + 3H_2O \rightarrow MoO_3(s) + 6H^+ + 6\ e^-$

$MoO_3(s) + H_2O \rightleftharpoons H_2MoO_4(aq) \cdots$ [42,43].

- **TiN:** $TiN(s) + 2H_2O \rightarrow TiO_2 + 1/2N_2 + 4H^+ + 4\ e^-$

$TiO_2\ (s) + 2H_2O \rightleftharpoons Ti(OH)_4(aq) \cdots$ [44].

- **W:** $W(s) + 3H_2O \rightarrow WO_3(s) + 6H^+ + 6\ e^-$

$WO_3(s) + H_2O \rightarrow H_2WO_4(aq) \cdots$ [45].

- **Cu:** $2\ Cu(s) + H_2O \rightarrow Cu_2O(s) + 2H^+ + 2\ e^-$

$Cu_2O(s) + 2H^+ \rightleftharpoons 2\ Cu^+ + H_2O \cdots$ [46,47].

For Mo and W, oxidizing environments favor soluble molybdate, tungstate, or peroxometal species, resulting in continuous oxide dissolution once passivation is disrupted. TiN undergoes anodic oxidation to TiO_2, but hydrated Ti(IV) species remain stable under both acidic and alkaline cleaning conditions, limiting sustained passivation. In Cu, oxidants such as H_2O_2 accelerate anodic dissolution, while chloride or ammine complexation suppresses redeposition and sustains metal loss.

From a thermodynamic perspective, these behaviors reflect the fact that practical wet cleaning operating windows lie outside the passive stability domains defined by Pourbaix diagrams. Elevated solution potentials imposed by H_2O_2 shift metal–oxide–aqueous equilibria toward high-valent dissolved species. For Mo and W, the passivation domains of MoO_3 and WO_3 are narrow under acidic oxidizing conditions, whereas TiN oxidation intersects regions where hydrated Ti(IV) species are thermodynamically stable in solution. Cu exhibits an inherently limited Cu_2O stability window at high potentials, with ligand complexation further stabilizing dissolved Cu^+/Cu^{2+} species. As a result, oxide formation and dissolution may proceed concurrently, rendering passivation kinetically limited rather than thermodynamically stable during wet cleaning.

Localized corrosion is frequently observed in metals such as Al and Cu, where chloride ions penetrate passive films and initiate pit formation at defect sites [48,49]. Once nucleated, local acidification and oxidant availability accelerate pit propagation, whereas Mo and W more commonly undergo uniform dissolution when passivation fails [50]. These effects are further intensified by post-CMP residues, including trapped oxidizers or abrasives, particularly in recessed features such as trenches and vias, where incomplete removal can lead to delayed corrosion during subsequent processing. In addition, galvanic corrosion represents a critical failure pathway in semiconductor stacks: when dissimilar metals such as Cu/W or Mo/TiN are electrically coupled in oxidizing solutions, potential differences drive preferential dissolution of the less noble metal, while cathodic reactions are sustained on the more noble component [51,52]. This corrosion mode is highly localized, often initiating at interfaces, grain boundaries, or defects, and is especially severe in multilayer stacks such as TiN/W/Cu or TiN/Mo, with aggressive ions including Cl^-, F^-, and H^+ further exacerbating oxide breakdown and charge transfer [53–55].

The severity of corrosion during wet cleaning is strongly influenced by process and material factors. Elevated temperature and increased H_2O_2 concentration accelerate dissolution kinetics [56], while prolonged exposure, repeated cleaning cycles, or insufficient rinsing

Table 2
Summary of Corrosion Inhibition Effects of Various Inhibitors on Titanium-based nitrides Surfaces.

Inhibitor/ Coating Type	Conditions	Key Observations/ Results	Corrosion Inhibition Efficiency
AS-ALD (H_2-plasma pretreat on a-C)	Thermal ALD of TiN ($TiCl_4/NH_3$) at 390 °C on 45 nm a-C/Si_3N_4 patterns, 400 W H_2 plasma (20 s) used to suppress nucleation on a-C.	TiN nucleation is strongly suppressed on a-C; GPC is normal on Si_3N_4; exposure of defect sites is reduced.	Not specified [118]
AS-ALD with aromatic inhibitor (aniline) – ABCD super-cycle	PEALD TiN at 250 °C (TDMAT/ Ar–H_2 plasma) with ABCD–cycle including vapor–phase aniline inhibitor, patterns of Ru/Co vs SiO_2/Al_2O_3.	Inhibitor step blocks TiN nucleation on Ru/ Co while allowing growth on oxides; selectivity > 90% up to ~ 6 nm, unintended TiN exposure in galvanically sensitive regions is reduced.	Not specified [120]
HiPIMS-TiN coating (vs DCMS)	TiN (~1.25 μm) deposited on carbon steel by HiPIMS or DCMS, tested in 3.5% NaCl at 25 °C.	HiPIMS-TiN exhibited lower i_{corr}, more positive E_{corr}, larger $R_{p,}$; smoother surface (Ra 15 nm vs. 32 nm), and denser columnar structure with (200) texture; superior passivation confirmed by Nyquist/Bode plots and Kramers–Kronig consistency.	< 99.89% (HiPIMS vs base)< 92.65% (DCMS vs base) [115]
CrN/TiN multilayer coating	1 μ m-thick CrN/ TiN multilayers (1:9, 3:7, 5:5) on 316 L SS via RF sputtering, tested in 1 M H_2SO_4 + 2 ppm HF at 70 °C.	Alternating CrN/TiN layers form interfacial barriers and tortuous diffusion paths that suppress electrolyte ingress; 1:9 coating showed the lowest i_{corr} (0.76 μA/cm^2), highest $R_{ct.}$	< 99.01% [122]
High-temperature vacuum break	TiN (<10 nm) deposited by metal organic CVD, samples exposed to air at different temperatures (20–140 °C) immediately after vacuum break.	High-temperature vacuum break promotes TiO_2 surface formation; suppressing oxygen diffusion, resistivity increases over 750 h reduced from ~ 27% to ~ 17% compared to low-temperature exposure.	Not specified [114]
Ultrathin PEALD-TiN	TiN thickness 25–67 nm, TDMAT at 200 °C or $TiCl_4$ at 350 °C, tested in 0.05 M H_2SO_4 + 2 ppm HF at 70 °C.	TDMAT-TiN forms a ~ 5 nm amorphous interface layer that suppresses corrosion and reduces low interfacial contact resistance; $TiCl_4$-TiN shows pinholes and Cl-related defects.	Not specified [121]
Interfacial passivation — Y_2O_3 (0.5–1.0 nm)	ZrO_2 thin film (4–15 nm) on TiSiN electrode with 0.5–1.0 nm Y_2O_3 interlayer, ALD at 300 °C.	Y_2O_3 interlayer suppresses Si diffusion from TiSiN; eliminating Zr-silicate formation (from 3.66% to 0.0%), dielectric permittivity is retained and leakage current is significantly reduced.	Not specified [128]
HTO – TiO_2 shell	HTO at 250 °C for 24 h in pure water, tested in 0.5 M H_2SO_4 + 0.05 wt% F^-.	Formation of anatase nanoparticle layer (~20 nm) creates coherent interface with TiN; oxide film remains intact and prevents pitting and intergranular corrosion.	Not specified [129]
HTO on MAIP-TiN	HTO in pure water at 200–250 °C for 24 h, TiN coated via MAIP.	Formation of compact anatase nanoparticle shell (~20–50 nm thick) on TiN surface suppresses corrosion current and broadens passivation range.	< 98.2 [130]
Glycine	0.3 wt% H_2O_2, pH 7.5, with 0–3 wt% glycine.	RR decreased from 1576 to 723 Å $min^{-}1$; SER decreased from 5.3 to 1.7 Å $min^{-}1$; i_{corr} decreased by nearly 10×; roughness decreases and planarization improves.	< 79% (at 3 wt % glycine) [134]

*Note: The corrosion inhibition efficiencies reported in this table are derived under varying experimental conditions (e.g., pH, temperature, and oxidant concentration) and are not directly comparable across different studies.

compound surface damage. High-aspect-ratio geometries promote retention of reactive species, and disruption of passivation layers by etching or mechanical stress exposes underlying metals to attack. Incomplete rinsing or drying can leave residual ions that destabilize surfaces during storage or subsequent thermal steps, making post-CMP cleaning particularly critical [57]. Overall, corrosion during semiconductor wet cleaning arises from the combined effects of electrochemical dissolution, aggressive solution chemistry, localized attack, and galvanic coupling, and its extent is governed by both the intrinsic stability of individual materials and their electrochemical interactions within multilayer stacks, underscoring the need for material-specific passivation and inhibition strategies (Table 3).

3. Molybdenum (Mo) corrosion and passivation strategies

Mo has attracted considerable attention as a key material in next-generation semiconductor devices due to its excellent electrical conductivity, high melting point, superior mechanical strength, and stability under plasma exposure. It is applied across a range of critical structures, including gate electrodes, contact metals, and reflective barriers. Particularly in highly integrated processes where low-resistance metals are required, Mo has emerged as a promising alternative to conventional W [58–60].

However, Mo is vulnerable to corrosion under oxidative and acidic wet cleaning conditions, which can significantly compromise interfacial reliability during subsequent deposition processes [61,62]. During wet cleaning, exposure to oxidizing solutions containing hydrogen peroxide, nitric acid, or phosphoric acid leads to rapid formation of various Mo oxides on the surface, such as MoO_3, MoO_2, and Mo_4O_{11} [39,63,64]. These oxides are generally poorly conductive and readily soluble in aqueous environments, resulting in continuous surface loss. MoO_3 is a water-soluble species with a relatively low pKa (~3.5), which promotes delamination during wet cleaning and increases surface roughness, thereby degrading process uniformity [65–67]. Such corrosion not only undermines electrical performance but also severely impacts long-term device reliability.

Table 3
Summary of Corrosion Inhibition Effects of Various Inhibitors on W surfaces.

Inhibitor/Coating Type	Conditions	Key Observations / Results	Corrosion Inhibition Efficiency
BTC	Post- CMPa cleaning, neutral and alkaline media.	Adsorbs on W; electrostatic interaction (N^{+}–W^{-}); initiates protective layer formation.	< 93.5% (pH 7)< 91.1% (pH 11) [126]
BTA	CVD-W wafers, tested in post- CMPa cleaning, aqueous solution, pH 3–5.9, with citric acid,	Adsorbs on W via triazole N atoms; coordination bonds form protective film.	< 93.7% [146]
TTA	polyacrylic acid.	Adsorbs on W, N + π-electron interactions; hydrophobic film.	< 94.8% [146]
BTA	WC-FJT and binder alloys, tested in 20% NaCl, pH ≈ 10, with 10 mM inhibitor.	Adsorbs on WC-based surface via triazole N atoms; forms protective film (mono-/multilayer).	< 34.3% [147]
Imidazoline		Hydrolyzes in alkaline solution; poor and inconsistent adsorption.	accelerated corrosion [147]
picolinic acid	Tested in CMPa (H_2O_2-containing slurry), pH 2.5.	Adsorbs on W oxide via pyridine N; forms coordination complex (covalent bonding); monolayer adsorption (Langmuir).	< 87.8% [148]
PEI	0.7 wt% TMAH, pH 7	Multisite adsorption of protonated amine groups from cationic polymeric PEI on WO_3-covered W inhibits charge transfer.	< 97% (1 mM PEI-1800) [149]
Lysine	Tested in CMPa (H_2O_2-containing slurry), pH 2.5.	Protonated –NH_2 groups electrostatically adsorb on negatively charged W surface, forms stable adsorption layer.	< 84.5% [150]
Leucine		Aliphatic amino acid; limited protonation; weak adsorption.	< 9.2% [150]
Glutamic acid		Acidic amino acid; partial protonation; weak adsorption.	< 17.9% [150]
Tannic acid	Tested in 10 wt% Acetic Acid solution	chemically adsorbed iron–tannate (Fe-TA) complex film	< 64% (20-hour immersion, at 10 wt% Tannic acid) [151]
Siloxane polymer film (organosilane + BTA + HEDP)	Tested in 3.5% NaCl (saline solution), long-term.	Hydrolyzed organosilane forms crosslinked Si–O–Si polymer film; BTA integrates via siloxane–azole fragments; HEDP promotes polycondensation.	< 91.4% (immersion, 60 min)< 96.7% (CPD, 5 min at 0.5 A/dm^2) [153]
SiON dielectric film	Wet cleaning solutions – SH (H_2SO_4/H_2O_2) – N,N-dimethylacetamide – AA-based.	Acts as a dielectric shielding layer, preventing plasma charge accumulation and stabilizing metal line profile; combined with wet cleaning to remove polymer residues.	Not specified With SiON, tungsten vias were preserved in all cases; AA + SiON: side erosion also protected [154]
Laser-ablated surface + fluorooxysilane modification	Contact with deionized water, saturated water vapor (100% RH, 5 days), cavitation erosion (270 min), oscillated sand abrasion (10 h), falling sand test (10 cycles).	Forms hierarchical micro/nanotexture with fluorooxysilane layer and retained superhydrophobicity and thermal stability.	Not specified [155]
Diamondoid phosphonate monolayer	Not mentioned.	Covalent bonding between phosphonate group and hydroxylated WO_3 surface; eliminates HCl, yielding stable P–O bond and W linkages.	Not specified [156]
Thermally induced WO_3 self-passivation	Oxidizing atmosphere (2% O_2/He), 1 bar, 500–900 °C	Real-time WO_3 growth on polycrystalline W with strong crystallographic orientation dependence; Phase evolution (o-WO_3 → t-WO_3)	Not quantified; evaluated via oxide growth kinetics and structural stability using in-situ ETEM [160]
Chemically induced WO_3 self-passivation	$Fe(NO_3)_3$ catalyst, tested in CMPa (H_2O_2-containing slurry), pH 2.3.	Fe^{3+} decomposes H_2O_2 → O_2 via Fenton reaction; O_2 oxidizes W to WO_3; thin, porous oxide at low conc., dense WO_3 film at higher conc.	Not specified but i_{corr} decreased, E_{corr} shifted positive with Fe$(NO_3)_3$ addition [161]
	$Fe(NO_3)_3$ and H_2O_2 mixed oxidants, tested in CMPa (H_2O_2-containing slurry), pH 2.	Mixed oxidants generate hydroxyl radicals (•OH), stronger than H_2O_2 alone; •OH oxidizes W rapidly to soft WO_3 film.	Not specified but i_{corr} and SER decreased, with $Fe(NO_3)_3$ addition [162]

*Note: The corrosion inhibition efficiencies reported in this table are derived under varying experimental conditions (e.g., pH, temperature, and oxidant concentration) and are not directly comparable across different studies.

3.1. Passivation strategies based on chemical corrosion inhibitors

To mitigate these challenges, extensive efforts have been devoted to organic ligand-based corrosion inhibitors, which suppress Mo corrosion primarily through strong surface adsorption and passivation film formation [68–71]. Organosulfur heterocyclic compounds such as thiourea- and thiadiazole- based derivatives have demonstrated high inhibition efficiency, governed by molecular functional groups and electron density distribution, as validated through combined experimental and theoretical studies by Mahmoud A. Ahmed and Prerna Tripathi [72,73].

Comparative evaluations of inhibitors relevant to Mo barrier layer processes have highlighted the superior performance of 3-amino-1,2,4-triazole (ATA) over benzotriazole (BTA), as evidenced by significantly reduced etch rates, positive shifts in corrosion potential, enhanced impedance response, and the formation of denser and more uniform passivation layers (Fig. 2(A)) [74].

Beyond single-component systems, composite inhibitor strategies have also been explored to address galvanic corrosion and polishing compatibility. Notably, the co-addition of BTA and potassium pyrophosphate ($K_4P_2O_7$) in H_2O_2-based alkaline slurries effectively minimized the Mo–Cu potential difference while maintaining comparable removal rates, thereby suppressing galvanic corrosion (Fig. 2(B)) [75]. Surface-sensitive XPS analyses further indicated stabilization of Mo through increased oxide fractions, suggesting that controlled oxide formation contributes to corrosion inhibition.

In parallel, growing attention has been directed toward environmentally benign amino acid-based inhibitors, including arginine, glycine, histidine, and methionine, which exhibit tunable inhibition performance under oxidative cleaning conditions [76–79]. Electrochemical analyses and density functional theory (DFT) calculations confirmed that electron-donating functional groups such as

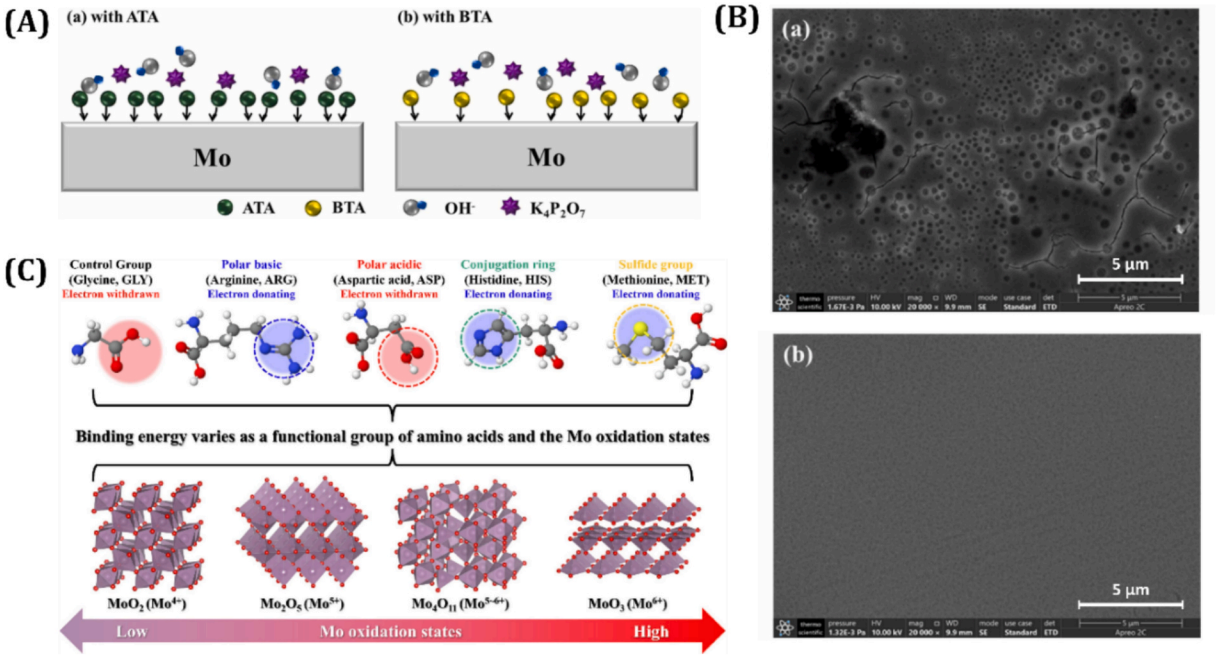

Fig. 2. (A) Molecular models illustrating the adsorption behavior of ATA and BTA on the Mo surface. [74], Copyright (2022) Elsevier. (B) SEM images of Mo wafers after immersion in 0.9 wt% H_2O_2 and 0.1 wt% $K_4P_2O_7$: (a) Reference and (b) Reference + 200 ppm BTA. The use of BTA clearly inhibits surface corrosion. [75], Copyright (2023) Elsevier. (C) Schematic of amino acid-based corrosion inhibitors with diverse functional groups, highlighting their role in stabilizing Mo oxides by preventing further oxidation of Mo^{6+} to MoO_3. [80], Copyright (2025) Elsevier.

guanidinium, imidazole, and thioether moieties promote stable adsorption on MoO_2 surfaces, preserving metallic Mo states and reducing dissolution (Fig. 2(C)) [80]. Comparative studies further revealed concentration-dependent inhibition mechanisms for glycine relative to BTA, emphasizing the role of surface complexation and zwitterionic interactions in regulating Mo oxidation and dissolution kinetics [81,82].

Additionally, antibiotic-derived molecules such as streptomycin have emerged as effective inhibitors in highly aggressive phosphate- and chloride-containing environments, forming protective surface layers that significantly reduce corrosion currents and hydrogen evolution [83].

Recent advancements in Mo corrosion control have been accelerated by the integration of machine learning-assisted screening [84,85]. By utilizing molecular descriptors and electronic properties (e.g., HOMO-LUMO energy, electronegativity) from diverse organic databases, machine learning models can predict the inhibition efficiency of new agents with high accuracy, significantly reducing the trial-and-error cycle in Mo-barrier slurry development [86,87]. Furthermore, to understand the transient dissolution of Mo at the nanoscale, in-situ characterization techniques such as in-situ EIS and operando flow-cell ICP-MS have been increasingly applied [88]. These methods allow researchers to monitor the real-time conversion of Mo to soluble peroxometallates under oxidizing conditions, providing precise kinetic data that traditional static etch tests cannot capture [89].

3.2. *Passivation strategies based on physical surface coatings*

In parallel with chemical control strategies employing organic and bio-derived inhibitors, as shown as Fig. 3(A), recent attention has been directed toward physically blocking Mo corrosion via the formation of nanoscale surface coatings [90–92]. Notably, chemical vapor deposition (CVD) based graphene coatings on Mo have been extensively investigated. Naghdi et al. demonstrated that graphene could be deposited onto Mo substrates under atmospheric conditions, and that the crystallinity of the graphene and the corrosion resistance of Mo could be enhanced by tuning the pre-annealing duration [93]. Extended annealing times promoted the formation of defect-minimized monolayer or bilayer graphene, significantly improving the initial corrosion resistance of Mo. However, upon prolonged exposure, the protective efficacy of the graphene films tended to converge irrespective of annealing, indicating a need for further studies to ensure long-term stability (Table 4).

In another study, Mo surfaces pretreated with nitric acid were coated with CVD grown graphene under varying hydrogen flow conditions. The results confirmed effective suppression of Mo oxidation even at elevated temperatures (300 °C) (Fig. 3(B)) [94]. Higher hydrogen flow rates reduced graphene defects and enhanced oxidation resistance, likely due to the reduction of the substrate surface during graphene growth, which facilitated the formation of a highly crystalline, electrochemically stable protective layer. Additionally, the growth of graphene on Mo substrates with a Pt underlayer has been proposed as a strategy to improve film quality [95]. The Pt-assisted approach enabled uniform bilayer graphene formation, markedly reducing surface oxide formation and enhancing corrosion inhibition. The Pt underlayer is thought to act catalytically, controlling nucleation and growth orientation, thereby improving the anti-corrosion performance of Mo. Collectively, graphene-based nanocoating complement the limitations of traditional chemical inhibitors, offering an advanced strategy for Mo corrosion mitigation while simultaneously providing excellent electrical, mechanical, and chemical stability.

Beyond graphene, substantial efforts have focused on applying metal oxide or composite ceramic coatings on Mo surfaces to inhibit oxidation and corrosion. For instance, glassy coatings incorporating ZrO_2 significantly improved Mo oxidation resistance under high-temperature conditions [96]. The increase in ZrO_2 content initially improved oxidation resistance; however, excessive addition resulted in a deterioration. Thermal treatment at 1300 °C resulted in a ~ 5-fold improvement in oxidation resistance, likely due to the formation of a viscous protective layer that improved adhesion to the Mo substrate.

Similarly, titanium–zirconium–molybdenum (Mo–Ti–Zr–C, TZM) alloys coated with $MoSi_2$-ZrB_2 composites exhibited exceptional protection even under 1600 °C oxidizing conditions [97]. This multilayer

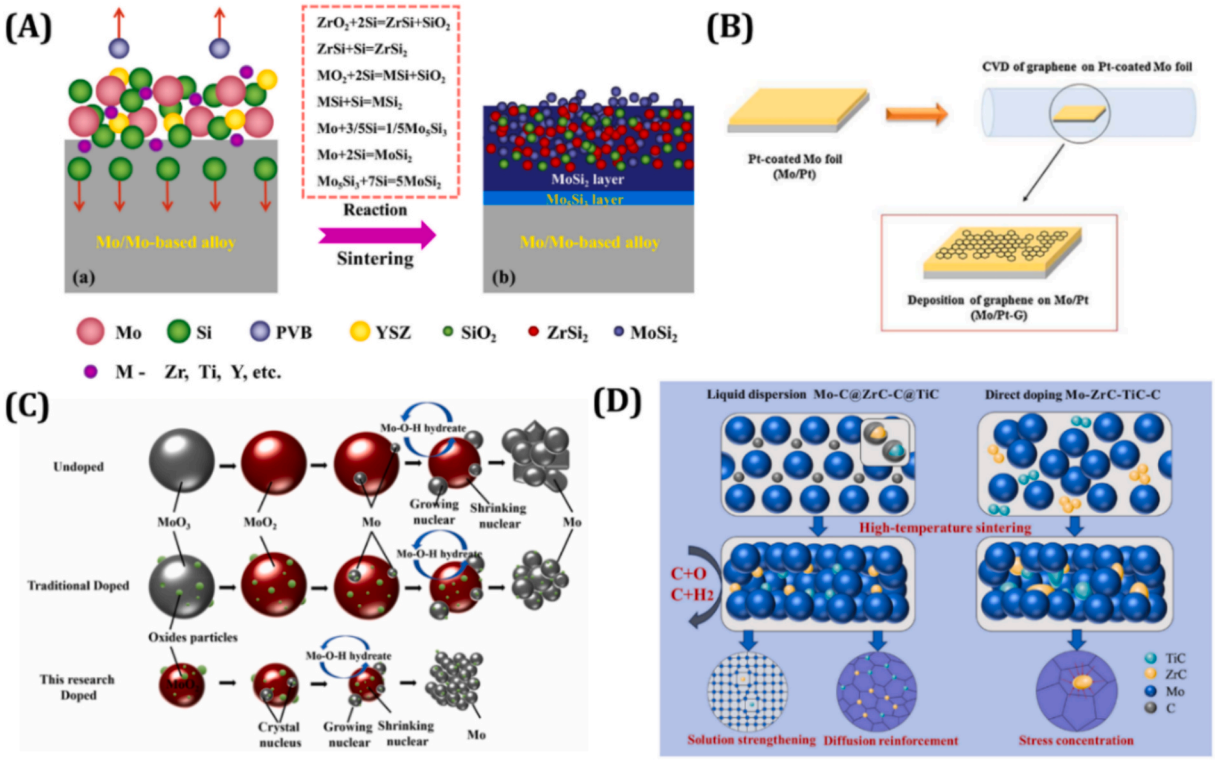

Fig. 3. (A) Schematic representation of the growth mechanism of slurry-sintered (SS) coatings on Mo and Mo-based alloys. [91], Copyright (2022) MDPI. (B) CVD of graphene on Pt-coated Mo (Mo/Pt-G). [94], Copyright (2018) Elsevier. (C) Schematic diagram of the Mo chemical vapor transport model. [98], Copyright (2024) Elsevier. (D)Illustration of the sintering behavior and oxygen removal processes occurring in Mo alloys that have been coated with a carbon layer. [99], Copyright (2025) Elsevier.

coating consisted of a MoB diffusion layer, a $MoSi_2$-ZrB_2 inner layer, and a SiO_2-ZrO_2 outer layer, forming a dense and stable $ZrSiO_4$-containing oxide scale that effectively blocked oxygen diffusion. Additionally, doping Mo alloys with ceramic oxide particles such as Al_2O_3 and Cr_2O_3 has been explored to simultaneously enhance high-temperature strength and oxidation resistance (Fig. 3(C)) [98]. These nanoparticles inhibit grain growth at boundaries and increase the mechanical strength of vacuum-sintered Mo alloys up to 862 MPa. Furthermore, Mo alloys with secondary TiC/ZrC carbide phases and carbon coatings demonstrated low oxidation susceptibility, excellent ductility, and elevated recrystallization temperatures, significantly improving mechanical stability under high-temperature conditions (Fig. 3(D)) [99]. Such enhancements in mechanical strength and oxidation resistance not only improve the durability of Mo alloys under extreme conditions but are also expected to contribute positively to corrosion mitigation during wet cleaning processes.

3.3. Technical limitations and failure mechanisms for Mo

Despite the effectiveness of current Mo passivation strategies, several inherent limitations remain that challenge their adoption in high-volume manufacturing. A primary concern is the occurrence of pore-driven localized attacks. While ALD or CVD-based nanocoating provides a physical barrier, sub-nanoscale pinholes can act as initiation sites for localized galvanic cells, leading to rapid lateral undercutting due to Mo's high sensitivity to dissolved oxygen [100–102]. Furthermore, Mo-oxides such as MoO_3 exhibit phase instability in alkaline media, being highly soluble in the aqueous environments typical of cleaning solutions. This can trigger a passivation-to-active transition, where the protective film itself dissolves and compromises surface integrity [40,80]. Finally, the thermal budget of organic inhibitors poses a significant hurdle; many inhibitors decompose during subsequent high temperature annealing steps, leaving carbon residues that degrade contact resistance and overall device reliability [81,103].

3.4. Summary and outlooks of Mo passivation

In summary, effective control of Mo corrosion in semiconductor processing has increasingly relied on a multifaceted framework that integrates chemical inhibition with nanoscale surface engineering. Organic, amino acid-based, and antibiotic-derived inhibitors enable chemically tunable passivation through tailored interfacial interactions, while graphene and ceramic nanocoating provide robust physical barriers against oxidation and dissolution. Together, these complementary strategies improve surface stability, suppress galvanic effects, and enhance process uniformity, thereby supporting the reliable integration of Mo in advanced device architectures. However, as device dimensions continue to shrink and process environments become more chemically aggressive, conventional empirical optimization approaches face intrinsic limitations, underscoring the need for more predictive, atomistical informed passivation design strategies.

Looking forward, the paradigm for Mo passivation is shifting from empirical screening toward atom-level control and AI-assisted material design. As semiconductor devices scale below 3 nm, achieving sub-nanometer uniform protection is critical to prevent the rapid dissolution of chemically unstable Mo oxides in aggressive cleaning media. Future research will increasingly rely on AI driven platforms that integrate deep learning with high-throughput DFT simulations to predict the precise binding energies and spatial orientations of complex organic inhibitors on Mo surfaces. This computational approach will be synergistically combined with advanced in-situ characterization, such as liquid cell TEM and operando EIS, to capture the transient conversion of Mo into soluble peroxometallates in real-time. Such atomic scale insights will enable the design of smart passivation layers capable of maintaining interfacial integrity even under fluctuating pH and temperature conditions in next-generation 3D structures.

Table 4
Summary of Corrosion Inhibition Effects of Various Inhibitors on Cu surfaces.

Inhibitor/Coating Type	Conditions	Key Observations / Results	Corrosion Inhibition Efficiency
BTA	B30 Cu-Ni alloy immersed in 2–10 g/L BTA solution in artificial seawater, pH 8.0, at 25–60 °C for 5–60 min.	Adsorbs on Cu, forms polymeric Cu(I)-BTA and chelated domains with Cu_2O, increasing surface hydrophobicity; acts as a mixed-type inhibitor blocking both anodic and cathodic reactions.	< 97.27% [182,183,185]
N1-CH_3-BTA	1 mM N1–CH_3-BTA in CMP slurry containing 5 wt % SiO_2 nanoparticles and 1.0 wt% H_2O_2.	Adsorbs onto copper surfaces via the triazole ring, forming a protective chemisorbed film that blocks active corrosion sites. The N1-methyl group can slightly increase steric hindrance, affect adsorption orientation but generally maintaining effective surface coverage.	< 96.4% [183]
N1–NH_2-BTA	1 mM N1–NH_2-BTA in CMP slurry containing 5 wt % SiO_2 nanoparticles and 1.0 wt% H_2O_2.	Adsorbing onto the metal surface via the triazole ring and amino group, forming a dense chemisorbed layer that blocks active sites for both anodic dissolution and cathodic oxygen reduction.	< 62.7% [183]
BTA + DA mixture	DA was applied to Cu (111) surfaces at 37 °C, 55 °C, and 80 °C with vapor pressures corresponding to 25–100% of saturation.	DA forms a protective hydrophobic film on Cu (111) surfaces via physisorption and van der Waals interactions, effectively reducing corrosion rates and increasing R_p, with inhibition efficiency increasing at higher surface coverage and temperature.	< 36.65% [184]
Water-soluble triazole derivatives (STR)	1 mM STR in 0.5 M NaCl solution at 25 °C.	Adsorbs onto copper surfaces via triazole N atoms and hydroxyl O atoms, forming chemisorbed protective layers.	< 92.73% [185]
AIA	2–10 mM AIA in aqueous solution under DFT and BOMD simulation conditions at 27–227 °C.	Can absorb at top, bridge, and hollow sites on Cu (100) surface in both perpendicular and parallel orientations, forming stable interactions via N atoms.	< 99.8% [186]
TEZ	CMPa slurry containing 0.4 wt% glycine, 0.5 wt% H_2O_2, and 1 wt% colloidal silica (60 nm), pH 9, with 2–10 mM TEZ.	Both chemical adsorption and physical barrier formation are possible due to electron-donating groups and π-bond structures.	< 97.6% [187]
MTEZ	CMPa slurry containing 0.4 wt% glycine, 0.5 wt% H_2O_2, and 1 wt% colloidal silica (60 nm), pH 9, with 2–10 mM MTEZ.	Methoxy groups can form hydrogen bonds, improving adsorption stability on the metal surface.	< 93.1% [187]
TAZ	CMPa slurry containing 0.4 wt% glycine, 0.5 wt% H_2O_2, and 1 wt% colloidal silica (60 nm), pH 9, with 2–10 mM TAZ.	Sulfur-centered strong adsorption forms a stable protective layer, especially effective in oxidative environments.	< 85.5% [187]
SHA	Varying concentrations of SHA containing 0.6 wt% H_2O_2, 1.2 wt% potassium tartrate, pH 9.	Capable of forming strong chemisorption on copper surfaces through coordination of oxygen and nitrogen atoms, potentially forming multiple surface bonds.	< 95% [188]
ATAH	0.001–0.01 M ATAH in 3.5% NaCl simulated seawater.	Adsorbs via N atoms on metal surfaces, forming stable coordination bonds; can interact with multiple surface sites.	< 98.28% [189]
MTAH	0.001–0.01 M MTAH in 3.5% NaCl simulated seawater.	Particularly effective in halide-containing or oxidative environments; inhibits both chemical and electrochemical corrosion.	< 92.49% [189]
FA	0.02–1.0 wt% FA in 0.2 M Na_2SO, pH 5.5.	Reduces corrosion by blocking active sites and chelating metal ions; effectiveness depends on concentration and pH.	< 87.1% [190]
Methionine	50 mM Methionine in the electrolytes comprising 1 wt% H_2O_2, pH 8.	Reduces corrosion of both Cu, with stronger adsorption ($\Delta G°_{ads}$ 23.9 kJ/mol), lowers CMP RRs, and promotes Cu(0)/Cu(I) preservation.	< 56.3% [191]
Leucine	50 mM Leucine in the electrolytes comprising 1 wt % H_2O_2, pH 8.	Inhibits Cu corrosion (η ~ 60%), slightly lowers Cu RR, and is easily removed during post-CMP cleaning.	< 61.2% [191]
Sol–gel S–N–C-doped TiO_2 nanocoating	S-N-C-doped TiO_2 nanocoating, tested in 3.5% NaCl at 200 °C.	Homogeneous, crack-free surface; chemical & physical protection.	< 99.6% [199]
Nanostructured ZrO_2 superhydrophobic coating	ZrO2@HMDS-coated copper via dip coating (2 cm × 2 cm) at room temperature, immersion 5 s, withdrawal 5 mm/s.	Provides both physical shielding and chemical stability; the high surface roughness combined with ZrO_2's chemical inertness prevents oxidation and corrosion.	< 99.96% [200]
SAM-based Elaidic acid (EA) polymer nanocoating	EA self-assembled and gamma-irradiated polymer nanocoatings on copper, tested in 0.2 g/L $NaHCO_3$, Na_2SO_4, $NaNO_3$	Acts as a molecular barrier, blocking the diffusion of corrosive species to the substrate; functional groups can also provide electrochemical stabilization.	< 95% [201]
N,S-CDs	N,S-CDs-modified copper in 0.5 M H_2SO_4 with 2–50 mg/L N,S-CDs for electrochemical tests at 25 °C.	High N/S content; chemisorption forms dense protective layer; compatible with downstream steps.	< 99.88% [202]
BTA-MOF/SiO_2 hybrid coating	BTA-MOF/silica-coated copper in 3.5 wt% NaCl after − 1.5 mA/cm^2 electrodeposition for 500 s.	Superhydrophobic (154.2° contact angle); maintains stable corrosion resistance for > 40 days.	< 99.6 [203]
CeO_2 nanocarrier self-healing coating	CeO2@BTA-silane-coated copper in 1 M NaCl after 1.3 V electrodeposition for 300 s.	Releases BTA at damage sites; regenerates protective layer.	< 99.7% [204]

*Note: The corrosion inhibition efficiencies reported in this table are derived under varying experimental conditions (e.g., pH, temperature, and oxidant concentration) and are not directly comparable across different studies.

4. Titanium-based nitrides corrosion and passivation strategies

Titanium-based nitrides, particularly TiN and TiSiN, are widely used in semiconductor processing as gate metals, contacts, interconnects, and diffusion barriers due to their excellent electrical conductivity, high hardness, and chemical stability [104–107]. TiN is established in complementary metal–oxide–semiconductor processes for polysilicon-gate compatibility [108] and stable interfaces with low-k dielectrics [109]. TiSiN is increasingly adopted in advanced nodes [110,111].

Nevertheless, thin TiN and TiSiN films can degrade under repeated oxidizing and acidic wet cleans and during ambient exposure at vacuum break [112–114]. At nanometer-scale thickness, surface roughening, and non-uniform passivation layers become major reliability concerns. TiN readily oxidizes in cleaning chemistries containing H_2O_2, O_3, or HNO_3 to form TiO_2 and TiO_xN_γ surface layers [112]. Prolonged exposure induces non-uniform oxide growth and increases localized pitting and dissolution. Oxide defects enable electrolyte penetration and form local galvanic couples, thereby accelerating corrosion. This is further promoted in fluoride-containing strong acids via soluble $[TiF_6]^{2-}$ formation and nitrogen depletion, leading to Ti-rich oxides (Fig. 4(A)) [115].

While the presence of Si in TiSiN improves overall oxidation resistance [110], hydrolysis of Si–O bonds and peeling of Si-rich phases can

occur in hot aqueous environments, particularly at 80–120 °C in H_2SO_4/H_2O_2 or SC-2 solutions [116]. In practical process, TiSiN gradually transforms to amorphous oxides (e.g., amorphous SiO_x or TiO_x), which limits its effectiveness as a diffusion barrier [117]. To mitigate these vulnerabilities while maintaining electrical performance, diverse passivation strategies for TiN and TiSiN have been proposed.

4.1. Passivation strategies based on deposition and microstructure

Atomic layer deposition (ALD) has emerged as a key approach to address these issues. ALD offers atomic-scale thickness control, excellent uniformity, and conformal coverage over complex 3D features. [118]. Stevens et al. used an H_2-plasma pretreatment to passivate amorphous carbon before $TiCl_4$/NH_3 TiN ALD at ~ 390 °C, suppressing TiN growth on a-C while maintaining normal growth on Si_3N_4 and achieving ~ 200:1 areal selectivity. By limiting deposition to target regions, selective ALD reduces exposed defect sites and indirectly lowers the risk of corrosion-prone exposure.

In fine-pattern processes, however, local selectivity can collapse at corners and edges with high curvature [118]. Self-assembled monolayer (SAM) inhibitors that form relatively stable films on flat surfaces can pack randomly or exhibit packing defects on complex nano geometries, facilitating unwanted nucleation [119]. To address this, an ABCD-type 'super-cycle' area-selective atomic layer deposition (AS-ALD) using periodic vapor-phase dosing of an aromatic inhibitor (aniline) has been proposed [120]. Merkx et al. implemented this strategy in plasma-assisted TiN ALD to achieve metal/dielectric selectivity and maintained > 90% selectivity even for ~ 6 nm-thick TiN films. The ABCD cycle consists of vapor-phase dosing of an aniline inhibitor (Step A), exposure to the Ti precursor tetrakis(dimethylamino)titanium (TDMAT) (Step B), Ar–H_2 plasma activation (Step C), and application of a substrate bias during the second half of the plasma step (Step D). Cyclic inhibition periodically refreshes inhibitor coverage and enhances reactivity contrast, suppressing local selectivity collapse and maintaining conformality in complex nano-patterns.

Alongside surface passivation, corrosion resistance in ALD-based films also depends on blocking internal percolation pathways via density control. Lee et al. reported that plasma-enhanced atomic layer deposition (PEALD) TiN films tens of nanometers thick exhibit increased E_{corr} and decreased corrosion current density (i_{corr}) under acidic conditions with F^- and/or elevated temperature, indicating improved corrosion resistance. The films also showed a low interfacial contact resistance (~15 mΩ·cm^2), satisfying both protective and electrical requirements (Fig. 4(B)) [121]. Similarly, high-power impulse magnetron sputtering (HiPIMS) can form dense microstructures by tuning ionization and substrate bias [115], which is reflected by higher polarization resistance (R_p) in EIS and by lower i_{corr} and more positive E_{corr} in potentiodynamic polarization (PDP) measurements. Compared with conventional direct current magnetron sputtering (DCMS), HiPIMS produces flatter, denser columnar films (Ra ≈ 15 nm, grain size ≈ 10 nm) relative to DCMS-TiN (Ra ≈ 32 nm, grain size ≈ 15 nm). These features hinder electrolyte infiltration and promote microstructure-driven passivation, substantially enhancing electrochemical stability.

In addition, multilayers such as CrN/TiN multilayers improve electrochemical corrosion resistance in simulated PEMFC electrolytes (1 M H_2SO_4 + 2 ppm F^- at 70 °C) [122]. The alternating layers distort diffusion pathways and introduce interfacial energy barriers, suppressing electrolyte ingress. For example, a CrN/TiN (1:9) stack exhibited a

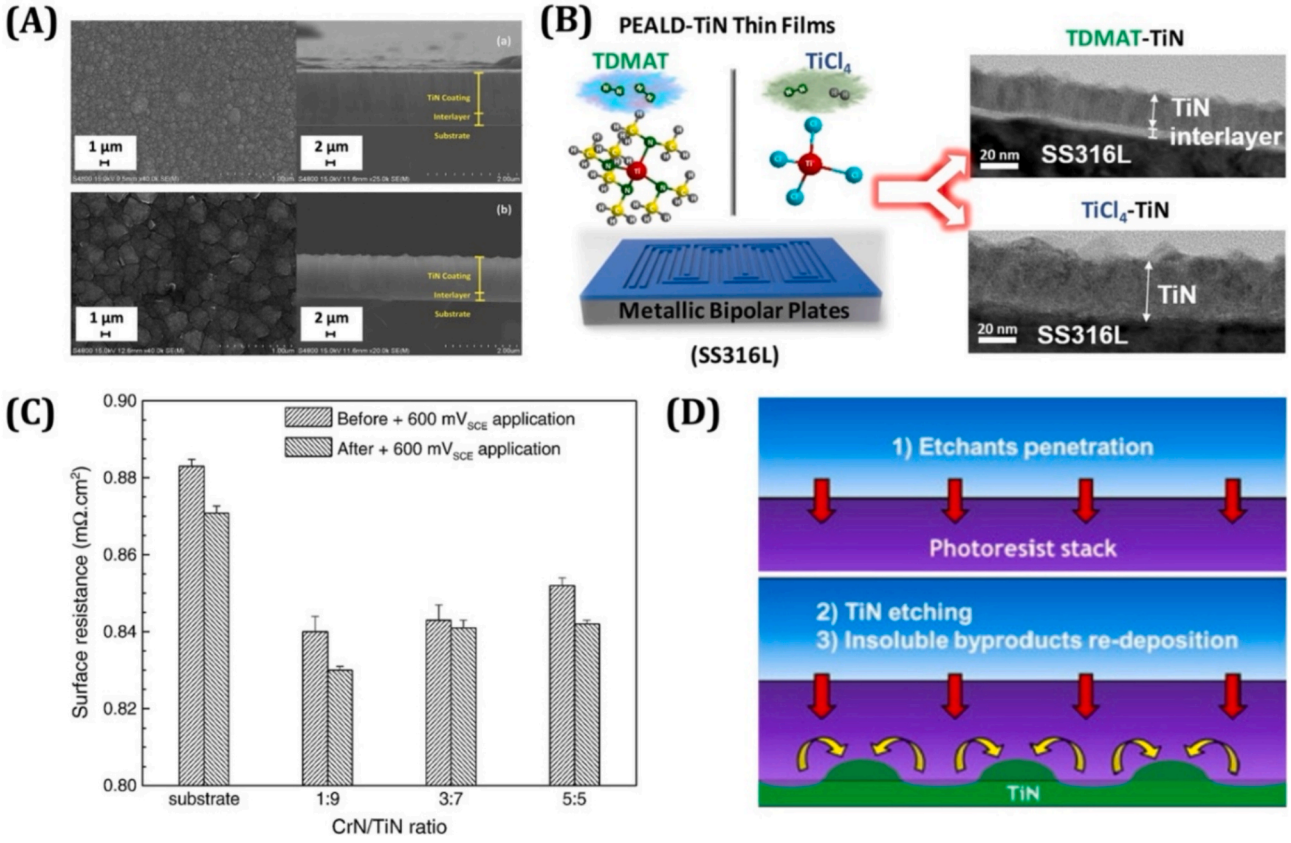

Fig. 4. (A) SEM micrographs of the TiN nanostructured coatings include both cross-section and top views of deposited coatings by HiPIMS and DCMS techniques. [115], Copyright (2017) Elsevier. (B) PEALD-TiN (TDMAT vs $TiCl_4$) on SS316L: process schematic, cross-sectional high-resolution TEM, and polarization in 0.05 M H_2SO_4 + 2 ppm HF at 70 °C [121], Copyright (2020) Elsevier. (C) CrN/TiN multilayers: Surface resistance of the specimens before and after the application of + 600 mV_{SCE} in a 1 M H_2SO_4 + 2 ppm HF solution. [122], Copyright (2011) Elsevier. (D) Proposed bumps formation mechanism from TiN oxidation, etching and re-deposition after SC1 diffusion through the PR. [123], Copyright (2015) Elsevier.

protective efficiency of 99.01% together with an increased charge-transfer resistance in polarization/EIS tests, supporting the synergistic role of multilayer interfaces (Fig. 4(C)) [122].

Amorphous oxide formed during the vacuum-break interval after deposition can also degrade interfacial reliability, motivating temperature-controlled strategies. Piallat et al. showed that controlling the vacuum-break temperature for metal organic CVD TiN limited the oxide thickness to 1.31 nm at 140 °C and reduced resistivity to 2.92 mΩ·cm, representing ~ 27% improvement relative to 20 °C [114]. These results suggest that controlling post-deposition exposure conditions can help suppress oxygen ingress and improve interfacial stability.

These studies indicate that ALD-based inhibitor strategies and surface passivation can work synergistically with the principle of blocking internal percolation pathways during semiconductor wet cleans. In practice, rather than eliminating all defects, it is often more practical and effective to design the system to remain in a stable passive-impedance state even when some defects are present.

In manufacturing, these strategies are often combined. Even under SC-1, stains or bumps can form on underlying TiN due to local chemistry changes coupled with sub-PR etching (Fig. 4(D)) [123]. In fin field-effect transistors, confinement alters ion distributions, making corners and edges prone to under-etch and non-uniform removal [113]. Under SC-1 (APM 1:4:20, 65 °C), TiN etching in confined nanoscale spaces can be up to ~ 38% faster than on planar regions, driven by double-layer overlap that enriches NH_4^+ and accelerates TiO_2 dissolution via rate-determining ammine complexation. A staged approach is therefore effective.

A dense, ultrathin PEALD TiN seed layer can block internal percolation paths and suppress attacks in stagnant zones. An auxiliary oxide passivation layer can be added when needed. Consistently, PEALD TiN maintains low i_{corr} values (<1 μA cm^{-2} in 0.05 M H_2SO_4 + 2 ppm HF at 70 °C) and reduced interfacial contact resistance, even with minor defects [121]. Overall, stack engineering is more practical than assuming defect-free films, as it sustains a high-impedance passive state despite limited defect exposure.

Recent TiN protection studies increasingly use machine-learning-guided process optimization to improve film quality through defect and microstructure control. A closed-loop Bayesian workflow for epitaxial TiN growth by MO-MBE identified suitable growth conditions after eleven growth experiments, illustrating accelerated process-window discovery for high-quality TiN films [124].

4.2. Passivation strategies based on interfacial and chemical control

In advanced semiconductor processing, corrosion is often governed by interfacial electrochemistry and galvanic coupling in multilayer stacks rather than by single-material passivation alone. Accordingly, stack potential design and electrochemical compatibility among adjacent materials are emerging as key levers for suppressing corrosion in Back End of Line environments. For example, in Cu/Ru/TiN barrier-liner stacks, potential differences can drive galvanic corrosion. As a system-level countermeasure, Sagi et al. developed a $KMnO_4$-based slurry formulation incorporating guanidine carbonate (GC) and 1 mM BTA, which reduced the galvanic potential differences (ΔE_{corr}) of both Cu/Ru and Ru/TiN couples to ~ 10 mV. This approach mitigates galvanic interactions not by directly enhancing intrinsic passivation of TiN, but by stabilizing the electrochemical balance across the stack under CMP-relevant conditions (Fig. 5(A)) [125].

Stack-level galvanic risks also arise in contact metallization, where Ti/TiN barrier liners can be galvanically coupled to neighboring conductors during post-CMP cleaning, motivating electrochemistry-aware chemistry design [126]. Moreover, TiN is itself a direct process surface, and CMP of TiN films using potassium permanganate with L-aspartic acid in alkaline slurry highlights that TiN surface reactions can be tuned through oxidizer–additive selection [127].

This potential-based concept also extends to TiSiN stacks, where long-term barrier integrity under hot aqueous conditions depends on interfacial stabilization. Jeong et al. inserted an ultrathin Y_2O_3 layer (0.5–1.0 nm) on TiSiN to suppress Si migration and interdiffusion at the TiSiN/ZrO_2 interface, eliminating Zr-silicate formation from 3.66% to 0.0% and improving leakage behavior while maintaining high permittivity in 4–5 nm dielectrics (Fig. 5(B)) [128]. This interfacial-stabilization approach relies on direct structural tuning and reactivity blocking, and is especially advantageous for long-term durability under hot, oxidizing conditions.

Meanwhile, hydrothermal oxidation (HTO) is an effective pretreatment to enhance the corrosion resistance of TiN/TiSiN films. Ren et al. formed a crystalline anatase TiO_2 nanolayer (~20–50 nm) on TiN using only water at 200–250 °C, with lattice registry between TiN (1 1 1) and anatase (004) that yields a robust interface (Fig. 5(C)) [129]. This coherent TiO_2 barrier blocks corrosive ingress and, in 0.5 M H_2SO_4 + 0.05 wt% F^-, increases E_{corr} and markedly reduces the corrosion rate. The 250 °C oxide remains protective during prolonged exposure, delaying TiO_2 dissolution to $[TiF_6]^{2-}$ and suppressing corrosion progression.

In addition, hydrothermal oxidation has been reported to markedly enhance the chemical stability of TiN films fabricated by multi-arc ion plating (MAIP), decreasing the i_{corr} by about 50 × relative to the untreated state and increasing the corrosion potential by more than 300 mV [130]. The concomitantly formed anatase TiO_2 nanolayer not only suppresses corrosion but also reduces frictional resistance, thereby improving wear resistance. Furthermore, a low-hazard partial-oxidation route using water and ozone partially oxidizes the TiN surface, increases hydrophilicity, and promotes surface cleaning, which strengthens both corrosion resistance [131].

Overall, hydrothermal and partial-oxidation pretreatments form dense, highly crystalline TiO_2 protection layers on TiN/TiSiN surfaces and deliver excellent corrosion inhibition in acidic and fluoride-containing environments. These approaches are practical and effective strategies for improving reliability and durability of TiN/TiSiN films in corrosive settings relevant to semiconductor processing and, separately, biomedical implants.

Interfacial pathways and chemical control are also emerging as key directions. Aberration-corrected environmental TEM directly resolved TiN oxidation evolution, showing initiation via Ti-atom migration along {200} and two vacancy-mediated pathways [132]. In situ EIS has been applied to TiN thin films, and EIS–microstructure analysis suggests that thickness alone cannot explain corrosion behavior, supporting real-time impedance metrics for tracking barrier degradation [133].

Finally, beyond physical protection layers, greener chemical additives can provide reaction-level control for suppressing TiN corrosion under oxidizing cleans. Cheng et al. quantitatively showed that adding glycine to the TiN–H_2O_2 system effectively suppresses oxidation and markedly reduces the corrosion rate (Fig. 5(D)) [134]. At 0.3 wt% H_2O_2 and pH 7.5, increasing glycine from 0 to 3 wt% reduced the removal rate (RR) from 1,576 to 723 Å min^{-1} and the static etching rate (SER) from 5.3 to 1.7 Å min^{-1}. The open circuit potential (OCP) stabilized rapidly, accompanied by an approximately ten-fold reduction in i_{corr}. EIS showed suppression of low-frequency diffusion features and an increase in low-frequency impedance, indicating a transition from diffusion-influenced behavior to charge-transfer-controlled kinetics.

4.3. Technical limitations and failure mechanisms for titanium-based nitrides

TiN passivation remains indispensable in advanced integration, yet its reliability can be constrained under contact-cleaning exposure and subsequent process conditions [135]. A central limitation is the non-uniform nature of oxidation. TiN oxidation has been reported to originate from Ti-atom migration along {200} planes and to proceed via vacancy-mediated routes that form either chains of titanium vacancies or staggered titanium vacancies, with reactivity varying with crystal orientation and surface curvature [132]. This microstructure

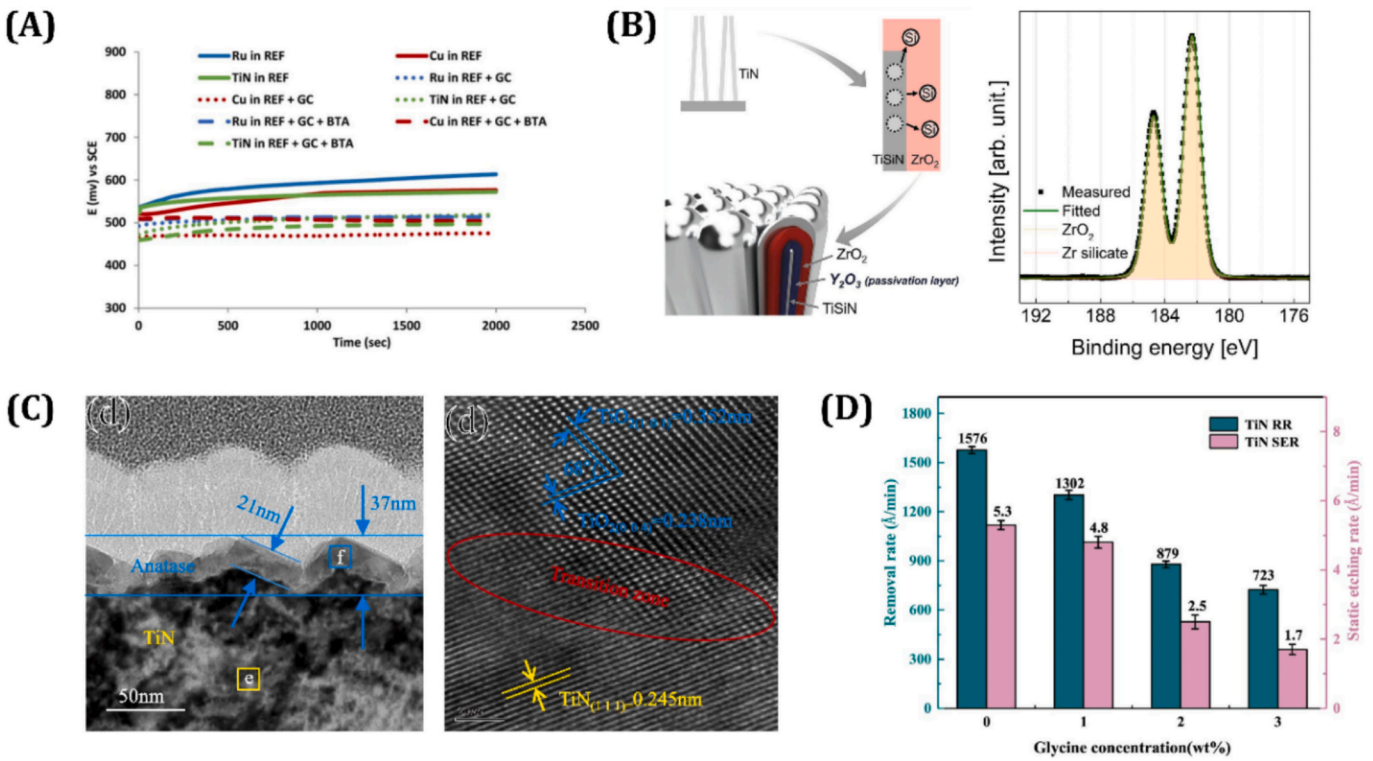

Fig. 5. (A) OCP of Cu, Ru and TiN in the presence of 10 mM $KMnO_4$ at pH 9 (REF), 10 mM $KMnO_4$ + 1 wt% GC at pH 10 (REF + GC) and 10 mM $KMnO_4$ + 1 wt% GC + 1 mM BTA at pH 10 (REF + GC + BTA). [125], Copyright (2016) ECS. (B) Y_2O_3 layer inserted between the ZrO_2 dielectric and the Ti(Si)N electrode blocks O/Si interdiffusion and suppresses Zr-silicate formation. Zr 3d XPS [128], Copyright (2020) Elsevier. (C) Cross-sectional STEM image of the HT-250 after HTO, showing a conformal anatase TiO_2 overlayer on TiN. [129], Copyright (2020) Elsevier. (D) Glycine effect on the TiN RR/SER in 0.3 wt% H_2O_2 at pH 7.5. [134], Copyright (2023) ECS.

dependence implies that, even under identical process conditions, oxidation resistance can vary locally, and passive-film breakdown may initiate preferentially at vulnerable sites [136]. From a stack perspective, relying on TiN alone as a diffusion barrier has been reported to be insufficient for suppressing dopant and contaminant transport under advanced integration conditions, underscoring the need for compositional and phase-structure control beyond conventional TiN [136]. Mechanical integrity also imposes a practical boundary, as TiN has been reported to exhibit lower hardness and reduced resistance to plastic deformation than TiSiN, such that accumulated local damage during processing can act as a weak point [137].

4.4. Summary and outlooks of titanium-based nitrides passivation

In summary, suppression strategies for titanium-based nitrides corrosion have evolved through a combination of deposition control, structural passivation, and chemical modulation. AS-ALD, aided by plasma pretreatments or vapor-phase inhibitors, confines TiN growth and minimizes exposure to corrosion-prone surfaces. Physical approaches such as hydrothermal oxidation and dense-film encapsulation further enhance stability by forming TiO_2-based shells and blocking percolation pathways. In TiSiN-based systems, ultrathin interlayers have been employed to mitigate silicate formation and preserve dielectric reliability under thermal and aqueous stress. Lastly, amino acid-based inhibitors can modulate interfacial redox reactions and suppress oxidation and etching under acidic and oxidizing conditions. Collectively, these strategies support reliable integration of TiN and TiSiN across wet cleaning and plasma-related steps. Continued progress will depend on hybrid schemes that combine spatial selectivity, interfacial robustness, chemical compatibility, scalability, and defect tolerance.

This effort will be enabled by atom-level oxidation diagnostics and in-situ monitoring that connect local microstructure and interfacial evolution to corrosion response. Atomic-scale observations of TiN oxidation can further guide microstructure-aware design rules that suppress vacancy-mediated reaction pathways at their earliest stages. In parallel, AI-assisted process optimization, such as closed-loop Bayesian approaches, provides a practical route to rapidly identify defect-minimizing growth windows and improve baseline film robustness prior to chemical exposure. Finally, translation of green inhibitor concepts to high-volume manufacturing will require demonstrating residue control, post-clean removability, and compatibility across full wet-clean sequences and downstream thermal budgets.

5. Tungsten (W) corrosion and passivation strategies

W is widely employed in semiconductor manufacturing owing to its high melting point and low electrical resistivity, which enable stable operation under severe thermal and electrical stress [41,138]. It is a key material for contact plugs and local interconnects and is further used as gate electrodes in 3D NAND word lines, buried word lines in dynamic random access memory cells, and through-silicon via interconnects [139–142], underscoring its central role in both logic and memory device architectures.

Despite these advantages, W is vulnerable to corrosion in semiconductor process environments. Exposure to oxidizing species such as H_2O_2, in both acidic and alkaline chemistries, destabilizes protective oxide layers and can result in surface roughening, void formation, and even via failure. Corrosion-induced defects in W plug processes [143], layout-dependent electrochemical degradation, and wear-assisted corrosion during chemical mechanical planarization (CMPa) have all been reported [144]. Quantitative studies further demonstrate that H_2O_2 markedly accelerates W dissolution, reducing the activation energy from 46.2 kJ mol^{-1} in water to 26.4 kJ mol^{-1} in H_2O_2-containing solutions [145]. These findings have motivated extensive investigation

into effective corrosion suppression and passivation strategies for W.

5.1. Passivation strategies based on adsorption-controlled corrosion inhibitors

Among the various strategies under investigation, one widely adopted approach is the incorporation of chemical inhibitors to suppress W dissolution under process-relevant conditions.

Meethal et al. investigated benzethonium chloride (BTC) as a W corrosion inhibitor in tetramethylammonium hydroxide (TMAH)-based neutral and alkaline post-CMPa cleaning solutions (Fig. 6(A)) [126]. Electrochemical tests (PDP, EIS) and inductively coupled plasma optical emission spectroscopy showed that BTC lowered the etch rate from 0.275 to 0.018 Å/min at pH 7 and from 0.685 to 0.061 Å/min at pH 11, achieving > 90% inhibition efficiency. Surface analyses (contact angle > 100°, XPS) confirmed the formation of a hydrophobic protective film. The inhibition mechanism arises from electrostatic attraction between the BTC cation and the negatively charged W surface, coupled with hydrophobic tail packing that blocks oxidant access. This highlights BTC's potential as a highly effective additive for advanced W post-CMPa cleaning and corrosion control.

In addition to BTC, complementary studies have emphasized the protective role of triazole-based inhibitors containing aromatic rings. International Business Machines Corp. discloses post-CMPa cleaning formulations incorporating BTA, tolyltriazole (TTA), and related heteroaromatic analogs as W-specific inhibitors in alkaline environments, with recommended concentrations of 0.01–1 wt% to suppress dissolution while maintaining cleaning efficiency [146]. Similarly, Yao et al. demonstrated that BTA significantly reduced i_{corr} and total weight loss in WC-based composites exposed to saline silica slurries (Fig. 6(B)) [147]. SEM and Raman analyses confirmed that BTA adsorbed on worn WC surfaces, mitigating binder dissolution and carbide pull-out. These findings underscore the applicability of aromatic triazole derivatives for corrosion protection in W systems.

As an additional example of aromatic inhibitors, chelating agents such as picolinic acid have also been explored for W corrosion protection. Lee and Seo reported picolinic acid as an effective corrosion inhibitor for W in acidic, oxidizing environments (Fig. 6(C)) [148]. Adsorption isotherm studies showed that it formed a uniform monolayer on WO_3 surfaces, reaching saturation at 1.5 wt%. At this concentration, the dissolution rate decreased from 90 to 11 Å/min, and atomic force microscopy (AFM) and SEM analyses confirmed preservation of grain integrity with smoother surface topography. The inhibition mechanism was attributed to coordinate bonding between the pyridine group and WO_3, which blocked active dissolution sites and stabilized the surface.

Polyethyleneimine (PEI), as a polymeric additive, has been investigated in which multiple amine groups are incorporated along a single chain to enhance surface coverage and adsorption strength. Meethal et al. evaluated PEI as a corrosion inhibitor for W in post-CMP cleaning environments [149]. In aqueous neutral media, PEI exhibited inhibition, reducing W dissolution by approximately 70–76% at 1 mM. concentration. In TMAH-containing solutions (0.7 wt% TMAH, pH 7), over 90% inhibition efficiencies were achieved despite the aggressive nature of TMAH toward tungsten. EIS, XPS, and DFT analyses supported an adsorption-controlled mechanism in which PEI adsorbs onto WO_3-covered W via amine-mediated electron donation, forming a compact polymer layer that suppresses interfacial charge transfer and limits oxidant access.

Beyond synthetic inhibitors, amino acids have also been explored as environmentally benign alternatives for W corrosion suppression. Pan et al. investigated amino acids as inhibitors to suppress W dissolution in peroxide-containing acidic solutions (Fig. 6(D)) [150]. Lysine, leucine, and glutamic acid were tested using etch rate measurements, electrochemical analysis, and AFM, with lysine showing the strongest effect by lowering the dissolution rate from 45.9 to 7.1 Å/min and reducing surface roughness from 1.647 to 1.267 nm at 0.25 mmol/L. EIS confirmed that lysine formed a protonated adsorption layer on the negatively charged W surface, which suppressed peroxotungstic acid generation and mitigated localized etching. This adsorption-controlled passivation achieved inhibition efficiencies above 80%, highlighting lysine as a promising green corrosion inhibitor.

Polyphenolic inhibitors, exemplified by tannic acid, have been reported as bio-based green corrosion inhibitors for tungsten-containing materials, in addition to amino acids. Jia et al. investigated the corrosion behavior of a tungsten alloy, W18Cr4V, using acetic acid as the corrosive medium [151]. Weight loss measurements, PDP, and EIS revealed strong concentration dependence. Low tannic acid concentrations (1–3 wt%) accelerated corrosion, while higher concentrations (≥5 wt%) provided inhibition, reaching a maximum efficiency of approximately 64% at 10 wt% tannic acid. SEM/EDS and XPS analyses indicated that a chemically adsorbed iron-tannate complex film, thereby increasing the charge transfer resistance and reducing metal dissolution, suppressed the corrosion. Overall, effective inhibition by tannic acid in W systems requires sufficiently continuous film formation on W surface.

5.2. Passivation strategies based on protective surface films

Some studies have focused on utilizing these molecules not only for adsorption but also as building blocks for forming protective surface layers, thereby creating more stable passivation films. Si-based strategies have emerged, where silane coupling agents, silicone-containing dielectrics, or fluoro-silanes are employed to generate durable passivation layers on W surfaces.

Cataphoretic deposition (CPD) has been applied to W using organosilane–inhibitor aqueous suspensions, producing continuous, low-porosity films within 5 min, whereas shorter deposition times resulted in discontinuous island-type layers [152]. Building on this approach, Shapagina et al. fabricated siloxane hybrid films by combining 3-(methacryloyloxy)propyltrimethoxysilane with BTA and hydroxyethylidene diphosphonic acid (HEDP) (Fig. 7(A)) [153]. Crosslinking enabled siloxane network formation, while the inhibitors improved film stability. The resulting coatings showed higher R_p and improved barrier properties compared to immersion films, and surface damage remained below 0.5% after prolonged exposure to 3.5% NaCl, demonstrating the effectiveness of silane–inhibitor hybrid passivation layers for W.

Lee and Ni evaluated the effect of a silicon oxynitride (SiON) dielectric barrier on W corrosion during post-metal etch cleaning with three chemistries: a sulfuric acid/hydrogen peroxide mixture (SH), a N, N-dimethylacetamide–based alkaline solution with ammonium fluoride and polyethylene glycol ether, and an alcohol amine (AA) mixture containing hydroxylamine, dihydroxybenzene, and hydroquinone (Fig. 7(B)) [154]. Of these, the AA solution combined with SiON reduced etch rates to < 5 Å/min and preserved W vias with minimal residues and only slight sidewall erosion. SEM and TEM analyses confirmed that the barrier maintained via integrity, and the study further showed that the SiON film prevented charge-induced corrosion.

Kuzina et al. fabricated fluoro-silane hydrophobic films on W by combining nanosecond pulsed laser ablation to generate hierarchical roughness with subsequent vapor-phase deposition of methoxy-{3 [(2,2,3,3,4,4,5,5,6,6,7,7,8,8,8-pentadecafluorooctyl)-oxy]-propyl} silane [155]. The optimized coatings exhibited contact angles above 170° with roll-off angles near 1–2°, and remained stable under water vapor exposure, continuous droplet contact for over 50 h, and mechanical abrasion. Morphological and EDS analyses confirmed uniform fluoro-silane coverage on textured surfaces, with substrate pre-heating improving adhesion. These results indicate that such surface-engineered hydrophobic barriers effectively suppress moisture-driven degradation and represent a viable approach for enhancing W corrosion resistance.

Phosphonate bonding functionalizes WO_3 surfaces through covalent P–O bond and W linkages, which are stronger and more stable than thiolate–metal bonds. Li et al. demonstrated that diamondoid

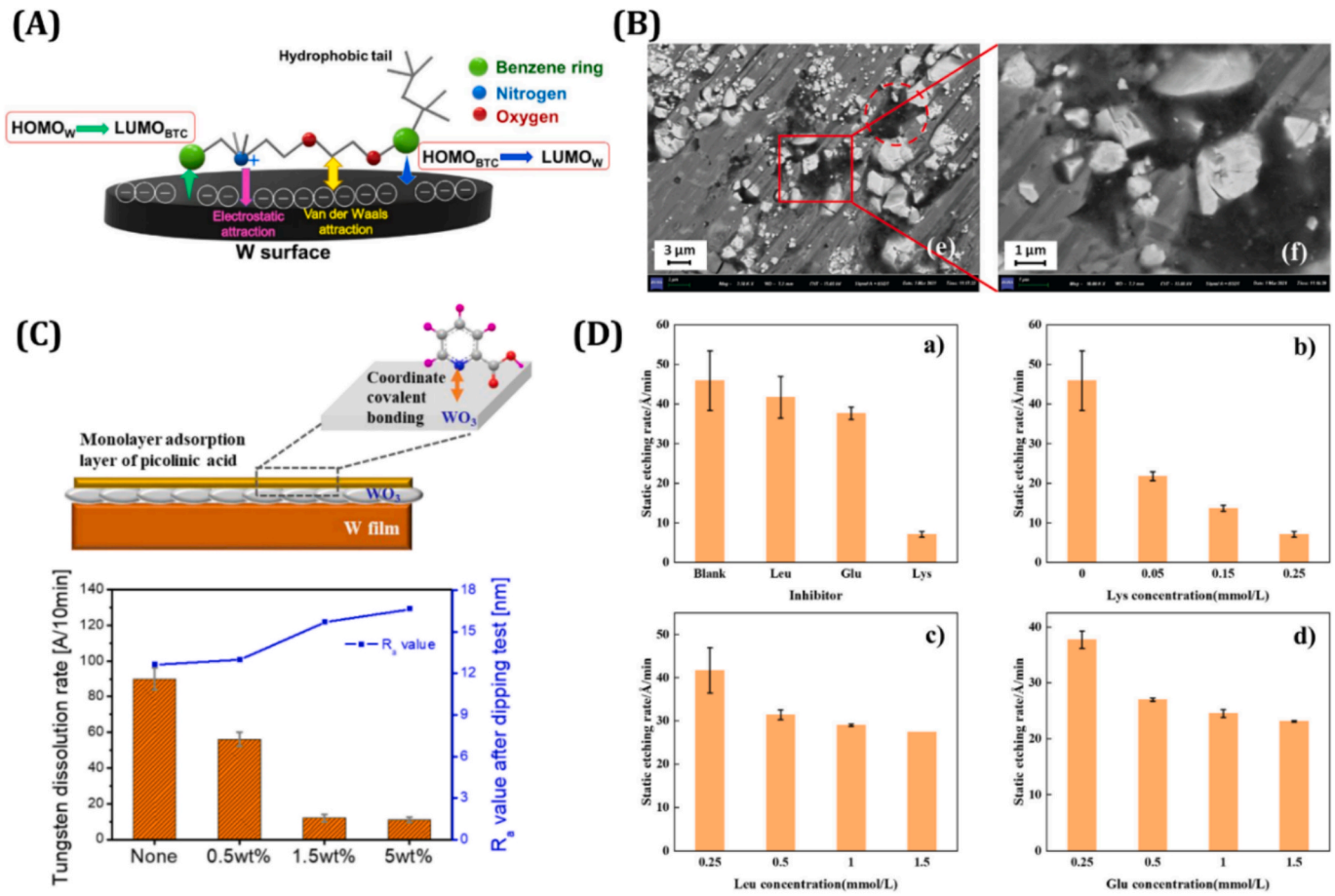

Fig. 6. (A) The schematic representation of the proposed model of corrosion inhibition by BTC on the W surface. [126], Copyright (2023) Elsevier. (B) SEM images of the worn surface of WC-FJT under different slurries: (e) IM slurry and (f) for the magnified SEM images of the corresponding rectangle regions. [147], Copyright (2021) Elsevier. (C) (a) Schematic illustration of picolinic acid adsorption onto the W films and (b) dissolution rate values from the W CMPa test for various picolinic acid concentrations. [148], Copyright (2022) MDPI. (D) (a) The SER with introduction of 0.25 mmol l − 1 amino acids; The SER with different concentrations of lysine (b), leucine (c) and glutamic acid (d). [150], Copyright (2024) The electrochemical society.

phosphonic dichloride monolayers remained intact up to 300–350 °C while passivating WO_3 against sublimation and degradation (Fig. 7(C)) [156]. The films also preserved the negative electron affinity of diamondoids, indicating that electronic properties were not compromised by the protective layer. These results suggest that phosphonate chemistry provides a stable route for constructing organic–inorganic barriers on W.

In addition to protective films derived from external materials, self-passivation approaches exploit W's inherent ability to form stable oxide layers under controlled chemical or electrochemical conditions. The resulting thin WO_3 film acts as an in-situ barrier that protects the underlying metal from dissolution, while remaining removable when required. [157–159].

Direct insight into the dynamic nature of tungsten self-passivation has been obtained using in situ environmental transmission electron microscopy (ETEM), as demonstrated by Togaru et al., which enables real-time observation of oxide film evolution under oxidizing conditions [160]. Using a gas-cell ETEM operated at 1 bar, WO_3 growth on polycrystalline W was visualized at 500–900 °C, revealing crystallographic orientation dependence and temperature-driven phase transitions from orthorhombic to tetragonal WO_3. While compact WO_3 layers initially formed and acted as diffusion barriers, elevated temperatures led to oxide sublimation and microcrack formation, resulting in passivation degradation. These observations demonstrate that WO_3-based self-passivation of W is inherently dynamic and structurally limited, providing a mechanistic basis for chemically stabilized passivation strategies.

$Fe(NO_3)_3$ has been applied as a strategy to control WO_3 passivation layers on W in acidic oxidizing solutions. Lim et al. showed that low $Fe(NO_3)_3$ concentrations produced porous WO_x with rapid dissolution, whereas higher concentrations promoted dense WO_3 films that reduced the etching speed by more than 80% [161]. Poddar et al. expanded this understanding by demonstrating that hydroxyl radicals generated in $Fe(NO_3)_3/H_2O_2$ mixtures drive rapid WO_3 growth, confirmed by spectroscopy and surface analyses (Fig. 7(D)) [162]. Their electrochemical tests showed a ~ 70% reduction in corrosion current and etching speed, underscoring that compact WO_3 passivation is the key mechanism suppressing W corrosion.

Xu et al. investigated the influence of solution chemistry on W stability during chemical-enhanced shear dilatancy polishing, emphasizing the role of controlled passivation [163]. By varying H_2O_2 concentration and pH, they assessed material removal, surface roughness, and electrochemical response. Excessive alkalinity or oxidant levels led to over-corrosion, whereas moderate conditions promoted uniform WO_3 film formation. Optimal stability was observed at pH 9 with 1 vol% H_2O_2, where dynamic WO_3 passivation provided both high removal efficiency and minimal roughness.

5.3. *Technical limitations and failure mechanisms for W*

Limited universality is a key limitation of W passivation, as inhibition depends strongly on solution chemistry and inhibitor concentration.

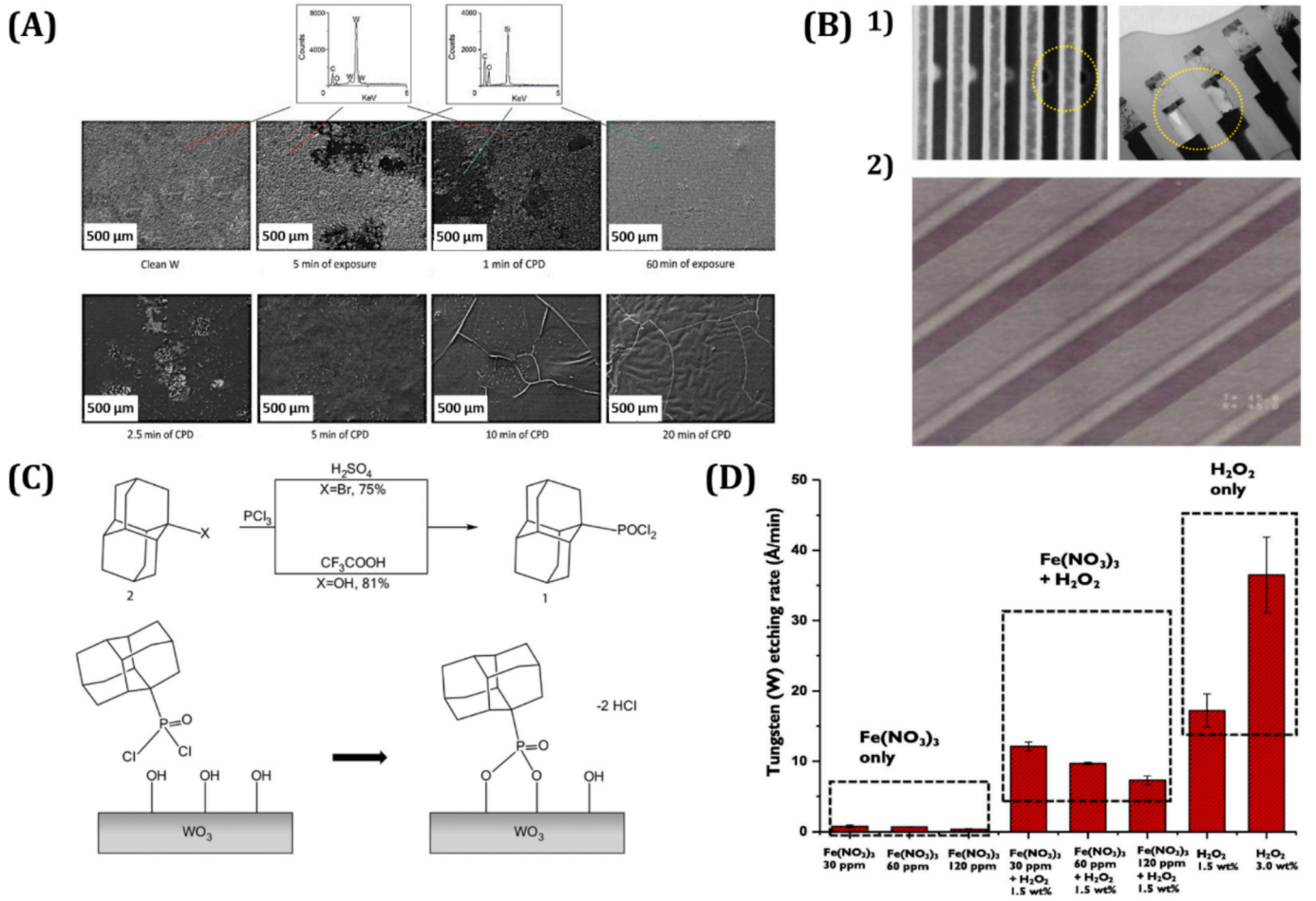

Fig. 7. (A) SEM images of films according to the duration of the CPD. [153], Copyright (2023) MDPI. (B) (1) Corrosion of W in vias (highlighted areas): top view and side view and (2) No residues or side erosion found in metal lines using solution AA with SiON. [154], Copyright (2010) Elsevier. (C) Proposed Reaction for the Synthesis and Attachment of 1-Dichlorophosphoryldiamantane (1) to a WO_3 Surface [156], Copyright (2013) American Chemical Society. (D) The change in W etching rate in the presence of single and mixed oxidizers of $Fe(NO_3)_3$, H_2O_2 and $Fe(NO_3)_3 + H_2O_2$ as a function of Fe $(NO_3)_3$ and H_2O_2 concentrations. [162], Copyright (2021) Elsevier.

PEI loses inhibition at highly alkaline pH under post-CMP conditions [149], while tannic acid exhibits concentration-dependent reversal in W systems, where low concentrations accelerate corrosion, highlighting narrow operating windows for passivation additives [151]. WO_x-based passivation is further limited by defect sensitivity: incomplete coverage and oxygen-vacancy engineering produce non-monotonic protection behavior, requiring controlled interfacial design rather than spontaneous oxide formation [164,165]. Under H_2O_2, WO_3 formation does not prevent corrosion, and increasing oxidant concentration exacerbates surface damage [166]. In addition, stability of WO_3 passivation layer is limited under alkaline conditions as W undergoes continuous anodic dissolution to soluble tungstate [167]. Microstructural heterogeneity also constrains passivation, as grain boundaries and secondary phases act as weak sites for localized attack [168]. Finally, galvanic coupling imposes a stack-level limitation because W is typically integrated with Ti/TiN liners; under post-CMP conditions, W–TiN coupling shifts mixed potentials and promotes preferential W dissolution despite nominal passivation or small-molecule inhibitor coverage, necessitating deliberate control of interfacial potentials and formulation chemistry beyond intrinsic W surface stability alone [169,170].

5.4. Summary and outlooks of W passivation

In summary, W corrosion mitigation can be broadly categorized into two main strategies: inhibitor-based chemical control and coating-based physical passivation. Inhibitor strategies include organic molecules, polymeric inhibitors, and environmentally benign green inhibitors, which suppress W dissolution primarily through surface adsorption and interfacial stabilization. Coating-based approaches—ranging from molecular-scale hybrids to dielectric barrier films such as Si-based barrier layers and phosphonate monolayers—provide physical separation between W surfaces and aggressive processing chemistries. Self-passivation via controlled formation of WO_3 layers has been investigated under regulated oxidizing conditions. These strategies mitigate W corrosion during CMP, wet cleaning, and post-etch processes by combining chemical inhibition with barrier protection. In industrial contexts, proprietary alkaline post-CMP cleaners incorporating organic inhibitors (e.g., Entegris AG-W100/CIP and ChemP) effectively suppress W corrosion while maintaining dielectric compatibility, confirming the practical viability of inhibitor-based strategies in semiconductor production environments [170,171].

Looking forward, machine-learning and AI-assisted screening are expected to complement—rather than replace—experimental workflows. Recent studies show that ensemble models and graph-based neural networks can predict corrosion-inhibition efficiency with high accuracy ($R^2 > 0.9$) when trained on harmonized datasets, enabling rapid pre-screening of candidate inhibitors and reducing experimental trial-and-error [87]. However, these approaches remain data-dependent and require rigorous electrochemical validation [172]. Future progress in W passivation will therefore rely on the synergistic integration of

machine-learning-guided screening, in-situ characterization, and targeted experiments to achieve predictive, mechanism-informed corrosion control.

6. Copper (Cu) corrosion and passivation strategies

Cu has been extensively employed as a critical material in semiconductor interconnect processes due to its low resistivity and excellent electron mobility. However, Cu is chemically susceptible and highly prone to corrosion during wet cleaning, interconnect, and capping processes. Under oxidizing cleaning solutions containing agents such as H_2O_2, O_3, or HNO_3, the Cu surface readily oxidizes and dissolves to form Cu^+ and Cu^{2+} ions [173,174]. Contact with liner metals including Ta/TaN, Co, or Ru further induces galvanic corrosion, accelerating selective material degradation. Such processes can lead to catastrophic defects including interconnect open circuits, increased resistance, and compromised device reliability. Therefore, to ensure the integrity of Cu interconnects in advanced semiconductor manufacturing, the implementation of effective passivation strategies grounded in a detailed understanding of the corrosion mechanisms is essential [175–177].

6.1. Passivation strategies based on chemical corrosion inhibitors

Traditionally, Cu corrosion inhibition has relied on azole-based organic passivators, most notably BTA, which adsorb on Cu surfaces to form protective films composed of Cu(I)–BTA complexes, chelated domains, and Cu_2O layers that block oxidant access [178–181]. This approach has demonstrated high inhibition efficiencies; for example, BTA treatment reduced the i_{corr} of a Cu–Ni alloy (B30) from 18.5 to 0.504 μA/cm^2 (97.27% efficiency), accompanied by increased surface hydrophobicity (contact angle: 85° → 102°) [182]. However, challenges remain in achieving uniform passivation within fine semiconductor features, as well as concerns regarding organic residues during subsequent processing.

To address these limitations, modified BTA derivatives and small heterocyclic inhibitors have been extensively explored. For instance, 1-methylbenzotriazol (N1-CH_3-BTA) enhances coordination with Cu through increased electron density, yielding denser protective films with reduced surface roughness (~0.923 nm) and improved inhibition efficiency (96.4%) (Fig. 8(A)) [183]. In addition, synergistic inhibitor systems, such as mixtures of BTA and decanoic acid (DA), have shown markedly enhanced performance by forming high-density protective layers via combined chemical and physical adsorption, achieving inhibition efficiencies up to 99.3% [184]. Such multicomponent strategies are particularly relevant to CMP and post-CMPa environments, where complex chemical interactions prevail.

Beyond classical BTA-based systems, next-generation heterocyclic inhibitors—including water-soluble triazole derivatives (STR), indazole-5-amine (AIA), tetrazole (TEZ), 5-methyltetrazole (MTEZ), and 1,2,4-triazole (TAZ)—have demonstrated strong Cu corrosion suppression under wet cleaning and alkaline CMPa conditions (Fig. 8(B)) [185–187]. These molecules typically adsorb parallel to the Cu surface and form polymeric or two-dimensional passivation layers through multiple coordination interactions, significantly lowering i_{corr} while increasing surface hydrophobicity. Notably, TEZ achieved an inhibition efficiency of 97.6% at 10 mM under strongly alkaline conditions, while maintaining a high Cu removal rate. More recently, salicylhydroxamic acid (SHA) has been reported to effectively mitigate Cu corrosion in peroxide-containing alkaline CMP slurries by forming hydrophobic protective films via combined physical and chemical adsorption [188].

Insights from chloride-containing environments further underscore the importance of molecular structure. For example, 5-aminotetrazole (ATAH) exhibited superior inhibition performance (98% at 0.01 M) compared to 5-mercapto-1-methyltetrazole (MTAH), attributed to enhanced electron donation from the amino group and stronger surface adsorption [189]. Although not yet directly implemented in CMP, such findings highlight the relevance of tailored heterocyclic chemistry for semiconductor cleaning environments.

Finally, environmentally benign inhibitors, including fulvic acid (FA) and amino acid–based compounds, have attracted growing attention (Fig. 8(C)) [190,191]. These inhibitors suppress Cu oxidation and dissolution through multidentate coordination involving carboxyl, hydroxyl, and amino groups, while offering advantages in sustainability and reduced residue-related risks during downstream processing.

While BTA has long been the industry standard for Cu passivation, recent research has shifted toward developing next-generation alternatives that overcome BTA's limitations, such as its environmental toxicity and potential for leaving organic residues. Nitrogen-free and advanced heterocyclic inhibitors, including various pyridine carboxylic acid isomers and tetrazole derivatives, have emerged as promising candidates. These molecules form stable hydrophobic layers through metal–organic coordination adsorption, achieving high inhibition efficiencies (≈98%) without the risk of nitrogen-related contamination, which is critical for maintaining dielectric integrity in sub-3 nm nodes [192].

Specifically, the structural dependency of these isomers and the density of the protective films formed by benzimidazole and its derivatives play a vital role in suppressing corrosion under alkaline environments [193]. Furthermore, organic phosphoric acid esters and chromium-free organic formulations have demonstrated effectiveness in creating robust inhibitory layers in neutral media, offering a more sustainable approach to Cu surface protection [194,195].

Furthermore, the adoption of bio-based corrosion inhibitors represents a significant step toward sustainable semiconductor manufacturing. Recent studies have demonstrated that amino acids—such as methionine, glutamic acid, and leucine—serve as environmentally friendly alternatives in CMP, providing corrosion protection for both Cu and Co surfaces [191]. Functional biomolecules like cysteine utilize multiple anchors to facilitate strong chemisorption on metal surfaces in both alkaline and neutral solutions [196]. By integrating these latest sustainable strategies, the industry is moving toward a more environmentally compatible yet technically rigorous approach to Cu corrosion control.

6.2. Passivation strategies based on physical and hybrid surface coatings

Beyond chemical inhibitors, nanocoating- and nanomaterial-based strategies have emerged as effective approaches for mitigating Cu corrosion in CMP and cleaning environments [197,198]. Unlike conventional adsorption-type inhibitors that provide only localized protection, nanoscale coatings enable uniform surface coverage while offering combined chemical and physical passivation. Representative examples include sol–gel-derived S–N–C-doped TiO_2 coatings and nanostructured zirconia-based superhydrophobic layers, which exhibit crack-free morphology, high contact angles (>150°), and corrosion resistance exceeding 99.9% under CMP-relevant conditions (Fig. 9(A)) [199,200].

In parallel, organic–inorganic nanocoatings such as SAM-based polymer films and N,S-codoped carbon dots (N,S-CDs) have demonstrated dense, chemically stable surface coverage through self-assembly and chemisorption mechanisms, achieving corrosion inhibition efficiencies above 95% and maintaining compatibility with downstream metallization processes [201,202].

More advanced hybrid strategies incorporate active corrosion inhibitors into functional host matrices. Notably, BTA-integrated metal–organic frameworks (MOFs) and CeO_2 nanocarrier-based self-healing coatings provide synergistic active–passive protection by combining superhydrophobic barrier layers with inhibitor release at damaged sites (Fig. 9(B), (C)) [203,204]. These hybrid nanocoating approaches enable long-term corrosion suppression while preserving process compatibility, positioning them as promising platforms for next-generation Cu interconnect protection.

The landscape of Cu passivation is being reshaped by the latest

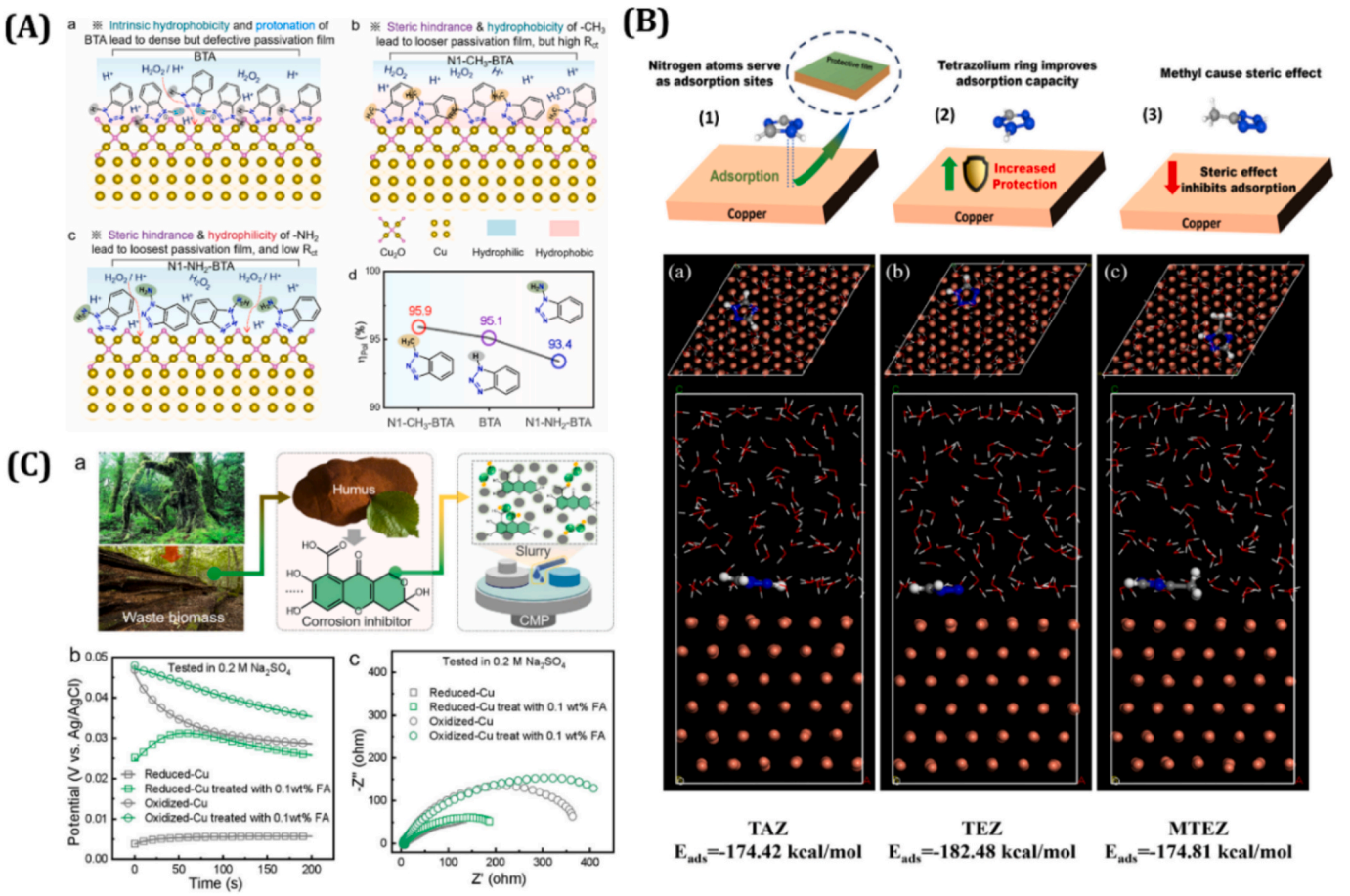

Fig. 8. (A). Schematic representation of passivation film formation on Cu surface by different BTA derivatives. [183], Copyright (2025) Elsevier. (B) The corrosion inhibition mechanism of TAZ, TEZ, and MTEZ in alkaline glycine medium was elucidated by analyzing their stable configurations on the Cu (111) surface at 1000 ps. [187], Copyright (2025) Elsevier. (C) Schematic diagram of the FA-derived CMPa slurry and electrochemical analysis of FA adsorption on reduced and oxidized Cu surfaces, including OCP and Nyquist plots from AC impedance tests. [190], Copyright (2025) Elsevier.

progress in green sustainable technologies, particularly the use of plant-derived extract inhibitors and bio-macromolecules [205,206]. These sustainable agents, such as polyphenols and humic substances, utilize multi-site coordination to form self-healing-like protective layers that are environmentally benign yet technically robust for sub-3 nm nodes [207]. To validate the integrity of these green barriers, in-situ TEM has become a vital tool, enabling the direct observation of passivation film growth and localized breakdown at grain boundaries during exposure to aggressive cleaning solutions. Additionally, hybrid strategies combining these green inhibitors with smart nanocarriers (e.g., CeO2 nano-containers) offer responsive protection [208], where inhibitor molecules are selectively released at damaged sites, as confirmed by high-resolution in-situ electrochemical mapping.

6.3. Technical limitations and failure mechanisms for Cu

Cu passivation techniques also encounter fundamental failure modes that limit their application in advanced interconnect architectures. A major issue is the trade-off between adhesion and electromigration performance. While strong chemical inhibitors, such as BTA derivatives, effectively prevent corrosion, they can leave organic residues that weaken the interfacial adhesion between the Cu surface and subsequent dielectric barriers, thereby accelerating electromigration failures [209,210]. In addition, galvanic breakdown remains a critical concern in complex 3D structures where Cu is in contact with noble liner metals like Ru or Co. If the passivation layer is not perfectly uniform, the electrochemical potential difference drives preferential dissolution at the Cu/liner interface [52,211]. Moreover, many thin-film strategies, including conventional SAMs, exhibit mechanical fragility during CMP, often lacking the robustness to withstand high shear stress, which results in passivation breakdown and localized pitting [212,213].

6.4. Summary and outlooks of Cu passivation

In summary, Cu corrosion inhibition strategies have diversified to include traditional chemical inhibitors (e.g., BTA, TAZ, STR, AIA), bio-based inhibitors (e.g., fulvic acid, amino acids), nanomaterials and nanocoatings (e.g., SAMs, graphene, h-BN, N,S-CDs), as well as MOF-based and self-healing hybrid coatings (e.g., BTA-MOF/SiO_2, CeO_2 nanocarriers). These approaches collectively provide chemical and physical protection across CMP, wet cleaning, metallization, and capping processes while maintaining surface uniformity and process compatibility.

Notably, nanomaterial-enabled and hybrid systems, particularly N,S-CDs and self-healing coatings, form dense and stable protective layers on Cu surfaces with high inhibition efficiency over a wide pH range [202]. However, most current strategies remain validated primarily at the laboratory scale, underscoring the need to address scalability, residue control, and long-term reliability under manufacturing-relevant conditions. This gap motivates the transition toward sustainable, manufacturable, and data-driven passivation concepts for advanced Cu interconnect technologies.

The future of Cu passivation lies in bridging the gap between innovative laboratory research and the feasibility of green inhibitors in

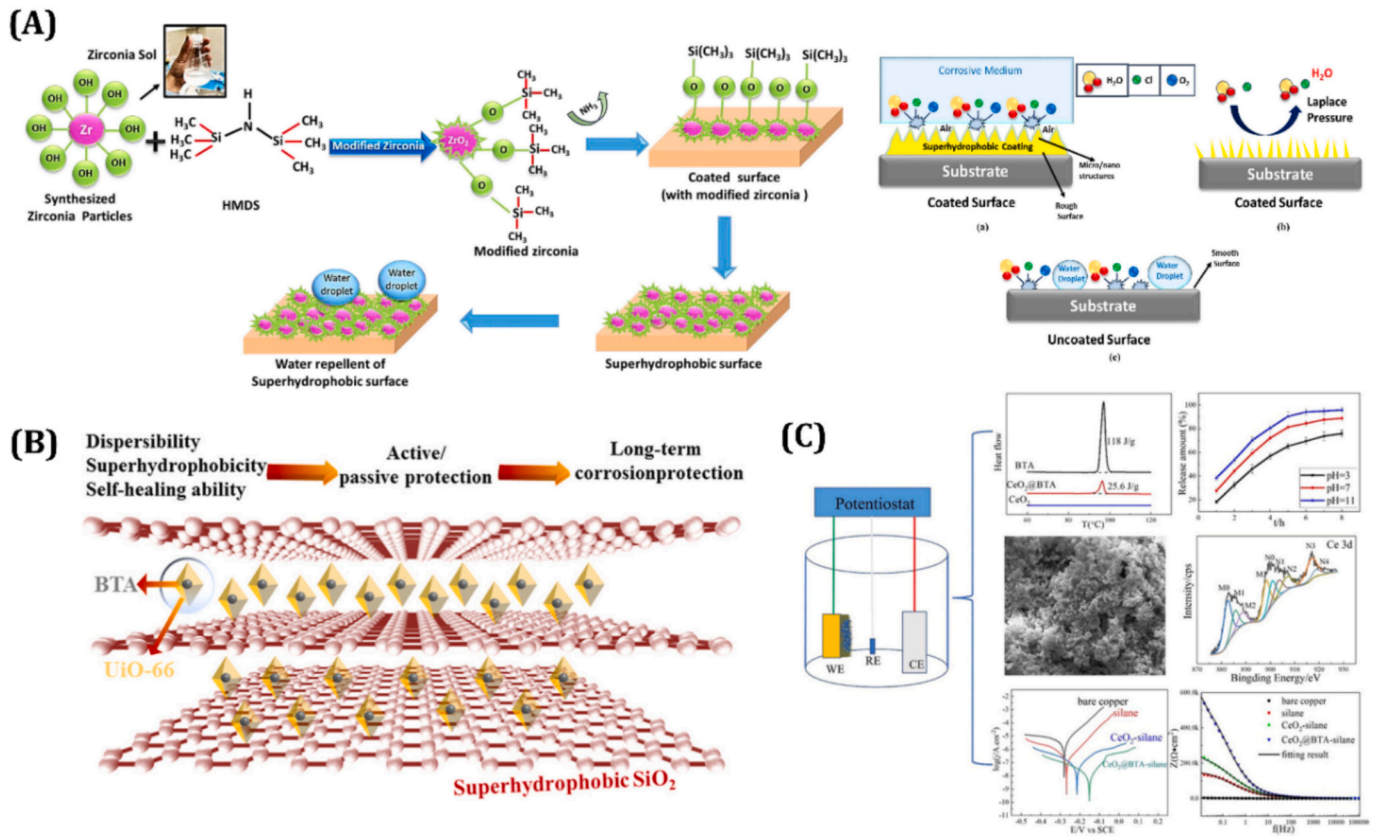

Fig. 9. (A) Modified zirconia coating confers superhydrophobic Cu with enhanced corrosion resistance by sustaining an interfacial air layer that impedes corrosive species. [200], Copyright (2025) Emerald. (B) Superhydrophobic BTA-MOF/SiO_2 coating delivers long-lasting active–passive corrosion protection on Cu. [203], Copyright (2024) Elsevier. (C) Hollow ceria-based smart coatings for enhanced corrosion protection on Cu. [204], Copyright (2024) Elsevier.

actual production lines. While bio-based macromolecules and plant-derived extracts offer promising eco-friendly alternatives, their transition to High-Volume Manufacturing requires a rigorous evaluation of their thermal stability and residue-free integration. Future studies must ensure that these sustainable inhibitors can withstand high-temperature annealing without degrading into carbonaceous defects that compromise interconnect reliability. Furthermore, AI-assisted design will be instrumental in selecting green molecules that exhibit high water solubility for efficient post-cleaning removal while providing superior chemisorption during CMP. Validating these sustainable strategies will rely on in-situ TEM and high-resolution electrochemical mapping to monitor localized breakdown at grain boundaries. Ultimately, the synergy between atomic-scale engineering and sustainable chemistry will establish a new paradigm for environmentally compatible and technically robust Cu corrosion control in advanced device architectures.

7. Conclusion

This review has systematically examined corrosion phenomena and passivation strategies for key metallic materials—Mo, W, titanium-based nitrides, and Cu—under semiconductor wet cleaning conditions. While these materials share common exposure to highly oxidative, acidic, or alkaline environments, their corrosion mechanisms and mitigation strategies differ substantially due to intrinsic physicochemical properties and device-level integration requirements.

Across all metals, several common challenges emerge: (i) the inability of native oxides to provide stable protection in aggressive cleaning chemistries, (ii) the increasing vulnerability of ultrathin films to localized electrochemical and galvanic corrosion, and (iii) the difficulty of achieving uniform passivation within complex three-dimensional nanostructures. These shared issues necessitate corrosion control strategies that are chemically robust, spatially uniform, and compatible with downstream processing.

At the same time, effective corrosion suppression requires differentiated, material-specific approaches. For Mo, the instability of high-valence oxides demands selective chemical inhibitors and electrochemical control strategies that suppress oxidative dissolution. W corrosion is dominated by rapid peroxide-driven oxidation, making dense physical barriers and film quality optimization essential. Titanium-based nitrides rely on maintaining oxide integrity and crystallinity to prevent localized degradation, highlighting the importance of deposition and post-treatment conditions. In contrast, Cu corrosion control must simultaneously address chemical dissolution and galvanic interactions, driving the development of advanced inhibitor systems, self-healing coatings, and hybrid MOF-based or nanoparticle-enabled passivation layers.

Recent advances indicate that corrosion control technologies are converging along three complementary pathways: chemical inhibition, physical protection, and hybrid strategies integrating both. Chemical approaches have evolved from traditional inhibitors toward highly selective molecules and environmentally benign alternatives, while physical strategies increasingly exploit advanced deposition techniques and nanostructured coatings. Hybrid systems, particularly for Cu interconnects, demonstrate strong potential by combining active corrosion suppression with mechanical robustness and self-repair capabilities.

In conclusion, ensuring the reliability of future semiconductor technologies requires an integrated corrosion management framework that accounts for both shared challenges and material-specific vulnerabilities. Future research should prioritize process-compatible, residue-minimizing passivation strategies capable of delivering atomic-scale uniformity and long-term stability within advanced 3D device architectures. The continued convergence of materials engineering,

electrochemical control, and sustainable chemistry will be central to establishing robust corrosion suppression paradigms for next-generation semiconductor manufacturing.

CRediT authorship contribution statement

Yejin Lee: Writing – original draft, Methodology, Formal analysis, Conceptualization. **Suyeon Bae:** Writing – original draft, Methodology, Formal analysis, Conceptualization. **Jee Woo Kim:** Writing – original draft, Methodology, Formal analysis, Conceptualization. **Byungjoon Kang:** Writing – review & editing, Validation, Investigation, Data curation. **Sungmin Kim:** Validation, Investigation, Data curation. **Jina Kim:** Validation, Investigation, Formal analysis, Data curation. **Insun Park:** Validation, Project administration, Funding acquisition, Conceptualization. **Kyu Young Hwang:** Writing – review & editing, Validation, Supervision, Project administration, Funding acquisition, Conceptualization. **Byung-Kwon Kim:** Writing – review & editing, Supervision, Resources, Project administration, Methodology, Investigation, Funding acquisition, Conceptualization.

Declaration of competing interest

The authors declare the following financial interests/personal relationships which may be considered as potential competing interests: Byung-Kwon Kim reports financial support was provided by Samsung Electronics Co Ltd. Byungjoon Kang reports financial support was provided by Samsung Electronics Co Ltd. Sungmin Kim reports financial support was provided by Samsung Electronics Co Ltd. Jina Kim reports financial support was provided by Samsung Electronics Co Ltd. Insun Park reports financial support was provided by Samsung Electronics Co Ltd. Kyu Young Hwang reports financial support was provided by Samsung Electronics Co Ltd. If there are other authors, they declare that they have no known competing financial interests or personal relationships that could have appeared to influence the work reported in this paper.

Acknowledgements

This work was primarily supported by Samsung Advanced Institute of Technology. This research was partially supported by the National Research Foundation of Korea (NRF) grant funded by the Korean government (MSIT and MOE) (No. RS-2025-16063688). Additional support was provided by the NRF grant funded by the Korean government (MSIT) (No. RS-2024-00351563) and by the Basic Science Research Program through the NRF, funded by the Ministry of Education (2021R1A6A1A10039823). This work was also supported by the Ministry of Trade, Industry & Energy (MOTIE, Korea) under the Industrial Technology Innovation Program (2410000556, Development of battery system technology to improve structure by applying heat transfer prevention technology).

Data availability

No data was used for the research described in the article.

References

[1] K.A. Reinhardt, R.F. Reidy (Eds.), Handbook for Cleaning for Semiconductor Manufacturing: Fundamentals and Applications, John Wiley & Sons, Hoboken, NJ, 2011.
[2] S. Singhal, B. Elkhatib, J. Stuber, S.V. Sreenivasan, O.A. Ezekoye, Characterization of wet batch cleaning process in advanced semiconductor manufacturing, IEEE Trans. Semicond. Manuf. 22 (3) (2009) 399–408, https://doi.org/10.1109/TSM.2009.2026321.
[3] W. Kern, Handbook of semiconductor wafer cleaning technology, Noyes Publication, New Jersey, 1993, p. 111.
[4] S.W. Lim, Control of SC1 wet cleaning process for nano-scale gate oxide integrity, Jpn. J. Appl. Phys. 42 (8R) (2003) 5002–5007, https://doi.org/10.1143/JJAP.42.5002.
[5] D.M. Knotter, The chemistry of wet cleaning, in: K.A. Reinhardt, R.F. Reidy (Eds.), Handbook of Cleaning in Semiconductor Manufacturing: Fundamentals and Applications, Wiley, Hoboken, NJ, 2010, pp. 39–94.
[6] E. Morita, H. Okuda, F. Inoue, K. Akiyama, Wet cleaning (Part 4): microroughness and COPs created by SC-1, in: Ultraclean Surface Processing of Silicon Wafers: Secrets of VLSI Manufacturing, Springer, Berlin, 1998, pp. 482–493.
[7] I.S. Cole, W.D. Ganther, J.D. Sinclair, D. Lau, D.A. Paterson, A study of the wetting of metal surfaces in order to understand the processes controlling atmospheric corrosion, J. Electrochem. Soc. 151 (12) (2004) B627–B635, https://doi.org/10.1149/1.1809596.
[8] G. Turner-Walker, The nature of cleaning: physical and chemical aspects of removing dirt, stains and corrosion. In Proc. Int. Symp. Cult. Herit. Conserv.; Tainan, Taiwan, (2012); pp 6–8.
[9] A. Conde, D. Macaya, J. De Damborenea, Corrosion of enamelled steel by domestic cleaning fluids, Br. Corros. J. 35 (4) (2000) 279–283, https://doi.org/10.1179/000705900101501344.
[10] D.S. Dunn, M.B. Bogart, C.S. Brossia, G.A. Cragnolino, Corrosion of iron under alternating wet and dry conditions. In CORROSION 1999; Association for Materials Protection and Performance: Houston, TX, 1999; pp 1–29.
[11] D.V.N. Vo, A.A. Adesina, Kinetics of the carbothermal synthesis of mo carbide catalyst supported on various semiconductor oxides, Fuel Process. Technol. 92 (6) (2011) 1249–1260, https://doi.org/10.1016/j.fuproc.2011.02.012.
[12] X. Zeng, X. Jiang, Y. Ning, Y. Gao, R. Che, Constructing built-in electric fields with semiconductor junctions and Schottky junctions based on Mo–MXene/Mo–metal sulfides for electromagnetic response, Nano-Micro Lett. 16 (1) (2024) 213, https://doi.org/10.1007/s40820-024-01449-7.
[13] G.L. Pearson, W.H. Brattain, History of semiconductor research, Proc. IRE 43 (12) (1955) 1794–1806, https://doi.org/10.1109/JRPROC.1955.278042.
[14] W. Lu, C.M. Lieber, Semiconductor nanowires, J. Phys. D Appl. Phys. 39 (21) (2006) R387–R406, https://doi.org/10.1088/0022-3727/39/21/R01.
[15] L.J. Brillson, The structure and properties of metal-semiconductor interfaces, Surf. Sci. Rep. 2 (2) (1982) 123–326, https://doi.org/10.1016/0167-5729(82)90001-2.
[16] M. Wittmer, TiN and TaN as diffusion barriers in metallizations to silicon semiconductor devices, Appl. Phys. Lett. 36 (6) (1980) 456–458, https://doi.org/10.1063/1.91505.
[17] H.I. Al Hossani, T.M.H. Saber, R.A. Mohammed, A.S. El Din, Galvanic corrosion of copper-base alloys in contact with molybdenum-containing stainless steels in arabian gulf water, Desalination 109 (1) (1997) 25–37, https://doi.org/10.1016/S0011-9164(97)00050-7.
[18] Y. Wang, H. Liu, C. Zeng, Galvanic corrosion of pure metals in molten fluorides, J. Fluorine Chem. 165 (2014) 1–6, https://doi.org/10.1016/j.jfluchem.2014.05.010.
[19] F.C. Chang, J.H. Beatty, M.J. Kane, J. Beck, Galvanic corrosion of tungsten coupled with several metals/alloys; ARL-TR-1845, U.S. Army Research Laboratory, Adelphi, MD, 1998.
[20] D.K. Merl, P. Panjan, J. Kovač, Corrosion and surface study of sputtered Al–W coatings with a range of tungsten contents, Corros. Sci. 69 (2013) 359–368, https://doi.org/10.1016/j.corsci.2013.01.002.
[21] G.L. Song, Effect of tin modification on corrosion of AM70 magnesium alloy, Corros. Sci. 51 (9) (2009) 2063–2070, https://doi.org/10.1016/j.corsci.2009.05.031.
[22] M. Mori, K. Miura, T. Sasaki, T. Ohtsuka, Corrosion of tin alloys in sulfuric and nitric acids, Corros. Sci. 44 (4) (2002) 887–898, https://doi.org/10.1016/S0010-938X(01)00094-4.
[23] J. Yang, Y. Song, K. Dong, E. Han, Research progress on the corrosion behavior of titanium alloys, Corr. Rev. 41 (1) (2023) 5–20, https://doi.org/10.1515/corrrev-2022-0031.
[24] Z. Song, S.P. Neo, C.K. Oh, S. Redkar, Y.P. Lee, Copper corrosion issue and analysis on copper damascene process, IEEE Trans. Device Mater. Reliab. 5 (2) (2005) 206–211, https://doi.org/10.1109/TDMR.2005.846826.
[25] L. Zhang, Y. Meng, Y. Xian, W. Zhang, H. Zhou, J. Fang, Y. Zhang, Copper corrosion issue analysis and study on advanced CMP process. In Proc. 2021 China Semicond. Technol. Int. Conf. (CSTIC); IEEE: Piscataway, NJ, 2021; pp 1–3.
[26] W. Qin, Corrosion mechanisms of copper and gold ball bonds in semiconductor packages: a unification of structure-based inference and electrochemical investigation, in: Advanced Driver Assistance Systems and Autonomous Vehicles: from Fundamentals to Applications, Springer, Singapore, 2022, pp. 581–629.
[27] W. Kern, The evolution of silicon wafer cleaning technology, J. Electrochem. Soc. 137 (6) (1990) 1887–1892, https://doi.org/10.1149/1.2086825.
[28] C.F. Tsang, K.-W. Lee, H.L. Chan, A study of post-etch wet clean on electrical and reliability performance of Cu low-k interconnections, Microelectron. Reliab. 45 (2005) 517–525, https://doi.org/10.1016/j.microrel.2004.07.007.
[29] S. Joshi, W.G. Fahrenholtz, M.J. O'Keefe, Electrochemical characterization of Al 7075-T6 surface oxide after alkaline cleaning and activation, Appl. Surf. Sci. 257 (2011) 1859–1863, https://doi.org/10.1016/j.apsusc.2010.08.126.
[30] N.G. Mistkawi, M.A. Hussein, M. Ziomek-Moroz, S.B. Rananavare, Corrosion behavior of copper thin films in organic HF-containing cleaning solution for semiconductor applications, J. Electrochem. Soc. 157 (1) (2009) C24–C29, https://doi.org/10.1149/1.3245999.
[31] R. Joyce, K. Singh, S. Varghese, J. Akhtar, Effective cleaning process and its influence on surface roughness in anodic bonding for semiconductor device

packaging, Mater. Sci. Semicond. Process. 31 (2015) 84–93, https://doi.org/10.1016/j.mssp.2014.11.002.
[32] P.J. Resnick, Cleaning Optimization for Reduced Chemical Usage; U.S. Department of Energy, 1996; OSTI Report No. 402307.
[33] D.M. Knotter, S. De Gendt, P.W. Mertens, M.M. Heyns, Silicon surface roughening mechanisms in ammonia hydrogen peroxide mixtures, J. Electrochem. Soc. 147 (2) (2000) 736–741, https://doi.org/10.1149/1.1393219.
[34] Z. Xiao, M. Xu, T. Ohgi, K. Onishi, D. Fujita, Removal of Si(111) wafer surface etch pits generated in ammonia–peroxide clean step, Appl. Surf. Sci. 221 (1–4) (2004) 160–166, https://doi.org/10.1016/S0169-4332(03)00876-6.
[35] R. Vos, M. Lux, K. Xu, W. Fyen, C. Kenens, T. Conard, P. Mertens, M. Heyns, Z. Hatcher, M. Hoffman, Removal of submicrometer particles from silicon wafer surfaces using HF-based cleaning mixtures, J. Electrochem. Soc. 148 (12) (2001) G683–G689, https://doi.org/10.1149/1.1413483.
[36] K. Choi, S. Ghosh, J. Lim, C.M. Lee, Removal efficiency of organic contaminants on Si wafer by dry cleaning using UV/O3 and ECR plasma, Appl. Surf. Sci. 206 (1–4) (2003) 355–364, https://doi.org/10.1016/S0169-4332(02)01215-1.
[37] B. Ashe, K.L. Marshall, C. Giacofei, A.L. Rigatti, T.J. Kessler, A.W. Schmid, A. Kozlov, Evaluation of cleaning methods for multilayer diffraction gratings, Laser-Induced Damage in Optical Materials: SPIE Proceedings 6403 (2007) (2006) 243–251, https://doi.org/10.1117/12.694884.
[38] K.M. Noh, E.K. Kim, Y.K. Lee, Y.M. Sung, Effect of post-CMP cleaning on electrochemical characteristics of Cu and Ti in patterned wafer, Korean J. Mater. Res. 19 (3) (2009) 174–178, https://doi.org/10.3740/MRSK.2009.19.3.174.
[39] W.A. Badawy, F.M. Al-Kharafi, Corrosion and passivation behaviors of molybdenum in aqueous solutions of different pH, Electrochim. Acta 44 (4) (1998) 693–702, https://doi.org/10.1016/S0013-4686(98)00180-7.
[40] F. Cicconi, A. Ubaldini, A. Fiore, A. Rizzo, S. Cataldo, P. Agostini, A. Pietropaolo, S. Salvi, V. Cuzzola, S.R.F. Collaboration, Dissolution of molybdenum in hydrogen peroxide: a thermodynamic, kinetic and microscopic study of a green process for 99mTc production, Molecules 28 (5) (2023) 2090, https://doi.org/10.3390/molecules28052090.
[41] S.H. Choi, M.E. Kreider, A.C. Nielander, M.B. Stevens, G. Kamat, J.E. Koo, K. H. Bae, H. Kim, I.Y. Yoon, B.U. Yoon, K. Hwang, Origins of wear-induced tungsten corrosion defects in semiconductor manufacturing during tungsten chemical mechanical polishing, Appl. Surf. Sci. 598 (2022) 153767, https://doi.org/10.1016/j.apsusc.2022.153767.
[42] V.P. Guro, Molybdenum dissolution in mixtures of H2O2 and concentrated HNO3 and H2SO4 in the presence of tungsten, Inorg. Mater. 44 (3) (2008) 239–243, https://doi.org/10.1134/S0020168508030059.
[43] X. Xia, W. Guan, G. Zhang, Q. Zhou, Q. Li, Z. Cao, S. Wu, Formation and stability of molybdenum and tungsten species in peroxy solution, J. Solution Chem. 52 (5) (2023) 551–569, https://doi.org/10.1007/s10953-023-01249-4.
[44] B. Avasarala, P. Haldar, Electrochemical oxidation behavior of titanium nitride based electrocatalysts under PEM fuel cell conditions, Electrochim. Acta 55 (27) (2010) 9024–9034, https://doi.org/10.1016/j.electacta.2010.08.035.
[45] M. Anik, K. Osseo-Asare, Effect of pH on the anodic behavior of tungsten, J. Electrochem. Soc. 149 (6) (2002) B224–B233, https://doi.org/10.1149/1.1471544.
[46] F. Habashi, Kinetics and mechanism of copper dissolution in aqueous ammonia, Ber. Bunsenges. Phys. Chem. 67 (4) (1963) 402–406, https://doi.org/10.1002/bbpc.19630670412.
[47] J.J. Fritz, Chloride complexes of copper(I) chloride in aqueous solution, J. Phys. Chem. 84 (18) (1980) 2241–2246, https://doi.org/10.1021/j100455a006.
[48] A.J. Sedriks, Corrosion of stainless steels, 2nd ed., Wiley, New York, 1996.
[49] G. Mankowski, J.P. Duthil, A. Giusti, The pit morphology on copper in chloride- and sulphate-containing solutions, Corros. Sci. 39 (1) (1997) 27–38, https://doi.org/10.1016/S0010-938X(96)00100-X.
[50] D. Narayanan, M. Liu, A. Martinez, R. Brooks, M. Kuttolamadom, H. Castaneda, Effect of Mo content on the passivation and localized corrosion behavior of laser engineered net shaped (LENS) Co-Cr-Mo alloys in a simulated physiological solution, Addit. Manuf. 77 (2023) 103812, https://doi.org/10.1016/j.addma.2023.103812.
[51] C.C. Hung, Y.S. Wang, W.H. Lee, S.C. Chang, Y.L. Wang, Galvanic corrosion between TaNx barriers and copper seed, Electrochem. Solid-State Lett. 10 (4) (2007) H127–H129, https://doi.org/10.1149/1.2437671.
[52] K. Lee, et al., Galvanic corrosion inhibition from aspect of bonding orbital theory in Cu/Ru barrier CMP, Sci. Rep. 11 (2021) 21214, https://doi.org/10.1038/s41598-021-00689-6.
[53] B. Avcı, K. Kazmanlı, B. Evren, M. Ürgen, Contribution of galvanic coupling with TiN, TiAlN, and CrN to the corrosion of steel in neutral and acidic chloride solutions, Mater. Corros. 74 (9) (2023) 1390–1399, https://doi.org/10.2139/ssrn.4384239.
[54] X. Cheng, C.J. Lin, Galvanic corrosion of TiN-W electro-couple during tungsten chemical mechanical polishing, J. Electrochem. 7 (2) (2001) 12–18, https://doi.org/10.61558/2993-074X.3250.
[55] K.A. Assiongbon, S.B. Emery, V.R.K. Gorantla, S.V. Babu, D. Roy, Electrochemical impedance characteristics of Ta/Cu contact regions in polishing slurries used for chemical mechanical planarization of Ta and Cu: considerations of galvanic corrosion, Corros. Sci. 48 (2) (2006) 372–388, https://doi.org/10.1016/j.corsci.2005.01.008.
[56] W. Li, B. Tan, S. Zhang, B. Gao, B. Ma, L. Guo, X. Wang, Application of an optimized alkaline cleaning solution for inhibitor removal during the Post-CMP process: performance evaluation and mechanism analysis, J. Mol. Liq. 369 (2023) 120892, https://doi.org/10.1016/j.molliq.2022.120892.
[57] C. Liu, R.I. Revilla, X. Li, Z. Jiang, S. Yang, Z. Cui, X. Li, New insights into the mechanism of localised corrosion induced by TiN-containing inclusions in high strength low alloy steel, J. Mater. Sci. Technol. 124 (2022) 141–149, https://doi.org/10.1016/j.jmst.2021.12.075.
[58] V.P. Kumar, D.K. Panda, Review—next generation 2D material molybdenum disulfide (MoS2): properties, applications and challenges, ECS J. Solid State Sci. Technol. 11 (3) (2022), https://doi.org/10.1149/2162-8777/ac5a6f.
[59] I.A. de Castro, R.S. Datta, J.Z. Ou, A. Castellanos-Gomez, S. Sriram, T. Daeneke, K. Kalantar-Zadeh, Molybdenum oxides - from fundamentals to functionality. Adv. Mater., 2017, 29 (40). DOI: 10.1002/adma.201701619 From NLM PubMed-not-MEDLINE.
[60] S. Tongay, D.S. Narang, J. Kang, W. Fan, C. Ko, A.V. Luce, K.X. Wang, J. Suh, K. D. Patel, V.M. Pathak, et al., Two-dimensional semiconductor alloys: monolayer Mo1−xWxSe2, Appl. Phys. Lett. 104 (1) (2014), https://doi.org/10.1063/1.4834358.
[61] Q.T. Le, H. Guevenc, A.U. Ibrahim, A. Klipp, S. Decoster, G. Murdoch, E. A. Sanchez, Wet cleaning of molybdenum for nano interconnects, ECS Trans. 108 (4) (2022) 39–44, https://doi.org/10.1149/10804.0039ecst.
[62] H. Cheng, B. Ma, L. Hu, S. Gu, Y. Xia, C.F. Hu, X.P. Qu, Controllable cyclic wet etching of molybdenum at room temperature, ACS Appl. Mater. Interfaces 17 (26) (2025) 38783–38796, https://doi.org/10.1021/acsami.5c09076 From NLM PubMed-not-MEDLINE.
[63] M. Bojinov, I. Betova, R. Raicheff, Transpassivity of molybdenum in H_2SO_4 solution, J. Electroanal. Chem. 381 (1–2) (1995) 123–131, https://doi.org/10.1016/0022-0728(94)03675-S.
[64] V.S. Saji, C.W. Lee, Molybdenum, molybdenum oxides, and their electrochemistry, ChemSusChem 5 (7) (2012) 1146–1161, https://doi.org/10.1002/cssc.201100660 From NLM Medline.
[65] S. Kim, Characterization of molybdenum compounds in aqueous solution, Texas A&M University-Kingsville, Kingsville, TX, 1999. Master's Thesis.
[66] M. Petrova, M. Bojinov, S. Zanna, P. Marcus, Mechanism of anodic oxidation of molybdenum in nearly-neutral electrolytes studied by electrochemical impedance spectroscopy and X-ray photoelectron spectroscopy, Electrochim. Acta 56 (23) (2011) 7899–7906, https://doi.org/10.1016/j.electacta.2010.12.022.
[67] Z. Li, Y. Lu, S. Zhang, X.W. Sun, T.Y. Dang, Z. Zhang, H.R. Tian, S.X. Liu, Triazole-modified molybdenum oxide with high proton conductivity, ChemistrySelect 5 (38) (2020) 11890–11895, https://doi.org/10.1002/slct.202003054.
[68] R.T. Loto, C.A. Loto, A.P.I. Popoola, Corrosion inhibition of thiourea and thiadiazole derivatives: a review, J. Mater. Environ. Sci. 3 (5) (2012) 885–894.
[69] J. Liu, Y. Chen, H. Wu, C. Ye, S.Z. Qiao, Anti-corrosive covalent iodo-thiadiazole catalyst enables Aqueous Zn horizontal line S batteries with high coulombic efficiency. .Adv Mater., 2025, e08570. DOI: 10.1002/adma.202508570 From NLM Publisher.
[70] H.S. Aljibori, O.H. Abdulzahra, A.J. Al Adily, W.K. Al-Azzawi, A.A. Al-Amiery, A. A.H. Kadhum, Recent progresses in thiadiazole derivatives as corrosion inhibitors in hydrochloric acid solution, Int. J. Corros. Scale Inhib. 12 (3) (2023) 842–866, https://doi.org/10.17675/2305-6894-2023-12-3-3.
[71] T.A. Nyijime, H.F. Chahul, A.M. Ayuba, F. Iorhuna, Theoretical investigations on thiadiazole derivatives as corrosion inhibitors on mild steel, Adv. J. Chem. A 6 (2) (2023) 141–154, https://doi.org/10.22034/AJCA.2023.383496.1352.
[72] M.A. Ahmed, S. Amin, A.A. Mohamed, Current and emerging trends of inorganic, organic, and eco-friendly corrosion inhibitors, RSC Adv. 14 (54) (2024) 31877–31920, https://doi.org/10.1039/d4ra05662k.
[73] P. Tripathi, R. Shakir, A.K. Verma, J. Karthikeyan, B. Ray, A.S.K. Sinha, S. Singh, Enhanced activity and chlorine protection in prolonged seawater electrolysis using MoS_2/sulfonated reduced graphene oxide, Sustainable Energy Fuels 9 (12) (2025) 304–321, https://doi.org/10.1039/d5se00541h.
[74] P. Wu, Q. Wang, W. Li, J. Ji, K. Zhang, Z. Ma, S. Wang, C. Wang, The study on corrosion inhibition effect of 3-amino-1,2,4-triazole and benzotriazole on molybdenum for barrier layer slurry, Colloids Surf. A 655 (2022) 130151, https://doi.org/10.1016/j.colsurfa.2022.130151.
[75] P. Wu, B. Zhang, Y. Shi, M. Xie, Y. Wang, D. Cui, M. Liu, W. Xian, Study on synergetic effect of potassium pyrophosphate and benzotriazole on chemical mechanical planarization of GLSI low-technology node molybdenum barrier layer, Mater. Sci. Semicond. Process. 168 (2023) 107830, https://doi.org/10.1016/j.mssp.2023.107830.
[76] L. Hamadi, S. Mansouri, K. Oulmi, A. Kareche, The use of amino acids as corrosion inhibitors for metals: a review, Egypt. J. Petrol. 27 (4) (2018) 1157–1165, https://doi.org/10.1016/j.ejpe.2018.04.004.
[77] H. Feng, L.-A. Cao, X.-P. Qu, Effect of Glycine on CMP Process of Molybdenum, in: Proceedings of the 2014 IEEE International Conference on Solid-State and Integrated Circuit Technology (ICSICT), Guilin, China, IEEE: Piscataway, NJ, 2014, pp. 1–3, https://doi.org/10.1109/ICSICT.2014.7021189.
[78] C.-H. Lee, H.-Y. Ryu, L. Teugels, K. Devriendt, H. Struyf, T.-G. Kim, J.-G. Park, Effect of corrosion inhibitors on chemical mechanical planarization of molybdenum. Proceedings of the International Conference on Planarization/CMP Technology (ICPT), 2021. Paper P6.
[79] K.Y. El-Baradie, N.A. El-Wakiel, H.A. El-Ghamry, Synthesis, characterization and corrosion inhibition in acid medium of *L*-histidine schiff base complexes, Appl. Organomet. Chem. 29 (3) (2015) 117–125, https://doi.org/10.1002/aoc.3255.
[80] S. Ryu, M. Moinpour, A. Rawat, P.J. Kim, E.J. Podlaha, J. Seo, Molecular interactions of amino acids for corrosion control in molybdenum CMP through bridging experimental insights and DFT simulations, Appl. Surf. Sci. 698 (2025) 163046, https://doi.org/10.1016/j.apsusc.2025.163046.
[81] S.-H. Choi, D.U. Lee, M.E. Kreider, M.B. Stevens, D. Park, I. Hong, K.-H. Park, K. Bae, H. Kim, B.U. Yoon, S.J. Kim, T.F. Jaramillo, K. Lee, Stabilization of

molybdenum in CMP: operando insights into distinct inhibitor adsorption pathways, J. Electroanal. Chem. 996 (2025) 119377, https://doi.org/10.1016/j.jelechem.2025.119377.
[82] G. Yang, P. He, X.-P. Qu, Inhibition effect of glycine on molybdenum corrosion during CMP in alkaline H_2O_2-based abrasive-free slurry, Appl. Surf. Sci. 427 (2018) 148–155, https://doi.org/10.1016/j.apsusc.2017.08.140.
[83] S.S. Medany, Y.H. Ahmad, A.M. Fekry, Experimental and theoretical studies for corrosion of molybdenum electrode using streptomycin drug in phosphoric acid medium, Sci. Rep. 13 (2023) 4827, https://doi.org/10.1038/s41598-023-31886-0.
[84] A. Hughes, D. Winkler, J. Carr, P. Lee, Y. Yang, M. Laleh, M. Tan, Corrosion inhibition, inhibitor environments, and the role of machine learning, Corros. Mater. Degrad. 3 (4) (2022) 672–693, https://doi.org/10.3390/cmd3040037.
[85] L.B. Coelho, D. Zhang, Y. Van Ingelgem, D. Steckelmacher, A. Nowé, H. Terryn, Reviewing machine learning of corrosion prediction in a data-oriented perspective, npj Mater. Degrad. 6 (1) (2022), https://doi.org/10.1038/s41529-022-00218-4.
[86] T.H. Pham, P.K. Le, D.N. Son, A data-driven QSPR model for screening organic corrosion inhibitors for carbon steel using machine learning techniques, RSC Adv. 14 (16) (2024) 11157–11168, https://doi.org/10.1039/d4ra02159b.
[87] K.M. Najam, A. Alshami, I.A. Hussein, Machine learning-driven prediction of corrosion inhibitor efficiency: emerging algorithms, challenges, and future outlooks, Arab. J. Sci. Eng. (2025), https://doi.org/10.1007/s13369-025-10386-5.
[88] B.M. Sultan, O. Gharbi, K. Ogle, J. Han, On-line inductively coupled plasma-atomic emission spectroelectrochemistry: real-time element-resolved electrochemistry, Curr. Opin. Electrochem. 41 (2023) 101350, https://doi.org/10.1016/j.coelec.2023.101350.
[89] M. Olgiati, M. Valtiner, Development of spectroelectrochemical microscopy for the real-time study of electrochemical surface processes, npj Mater. Degrad. (2025), https://doi.org/10.1038/s41529-025-00728-x.
[90] S. Richter, Concepts for novel oxidation resistant thin film materials; Doctoral Thesis, TU Wien, Vienna, Austria, 2025.
[91] T. Fu, F. Shen, Y. Zhang, L. Yu, K. Cui, J. Wang, X. Zhang, Oxidation protection of high-temperature coatings on the surface of Mo-based alloys—a review, Coatings 12 (2) (2022) 141, https://doi.org/10.3390/coatings12020141.
[92] J.H. Perepezko, T.A. Sossaman, M. Taylor, Environmentally resistant Mo–Si–B-based coatings, J. Therm. Spray Technol. 26 (5) (2017) 929–940, https://doi.org/10.1007/s11666-017-0565-2.
[93] S. Naghdi, I. Jevremović, V. Mišković-Stanković, K.Y. Rhee, Chemical vapour deposition at atmospheric pressure of graphene on molybdenum foil: effect of annealing time on characteristics and corrosion stability of graphene coatings, Corros. Sci. 113 (2016) 116–125, https://doi.org/10.1016/j.corsci.2016.10.012.
[94] S. Naghdi, K. Nešović, V. Mišković-Stanković, K.Y. Rhee, Comprehensive electrochemical study on corrosion performance of graphene coatings deposited by chemical vapour deposition at atmospheric pressure on platinum-coated molybdenum foil, Corros. Sci. 130 (2018) 31–44, https://doi.org/10.1016/j.corsci.2017.10.021.
[95] S. Naghdi, K.Y. Rhee, S.J. Park, Oxidation resistance of graphene-coated molybdenum: effects of pre-washing and hydrogen flow rate, Int. J. Refract. Met. Hard Mater 65 (2017) 29–33, https://doi.org/10.1016/j.ijrmhm.2016.11.008.
[96] Q. Wang, H. Wang, W. Ning, Influence of ZrO_2 on Oxidation resistant properties of glass-based coating on molybdenum substrate, Adv. Mater. Res. 160–162 (2011) 1762–1766, https://doi.org/10.4028/www.scientific.net/AMR.160-162.1762.
[97] Y. Zhang, X. Zhou, H. Cheng, Z. Geng, W. Li, Fabrication and oxidation resistance of a novel $MoSi_2$–ZrB_2-based coating on Mo-based alloy, Materials 16 (16) (2023) 5634, https://doi.org/10.3390/ma16165634.
[98] L. Yang, A. Si, S. Wei, X. Wang, Effects of Al_2O_3 and Cr_2O_3 on the microstructure and properties of Mo alloys prepared via vacuum sintering, Vacuum 225 (2024) 113230, https://doi.org/10.1016/j.vacuum.2024.113230.
[99] B. Hu, C. Quan, S. Ma, Q. Zhang, H. Xing, L. Wang, P. Hu, X. Zhou, Y. Li, X. Zhao, P. Feng, K. Wang, Strengthening–toughening mechanism of carbon-coated TiC/ZrC secondary phase doped molybdenum alloy, Mater. Sci. Eng. A 929 (2025) 148096, https://doi.org/10.1016/j.msea.2025.148096.
[100] E.O. Atofarati, P.O. Oviroh, O. Folorunso, T.C. Jen, Emerging applications and trends in atomic layer deposition nano-coatings, J. Coat. Technol. Res. 23 (1) (2025) 229–254, https://doi.org/10.1007/s11998-025-01154-z.
[101] M. Schneider, L. Šimůnková, A. Michaelis, W. Hoogsteen, Electrochemical machining of molybdenum, Int. J. Refract. Met. Hard Mater 101 (2021) 105689, https://doi.org/10.1016/j.ijrmhm.2021.105689.
[102] D.A. Shifler, LaQue's handbook of marine corrosion, John Wiley & Sons (2022) 63–121.
[103] K.U. Gamagedara, D. Roy, Mechanisms of chemically promoted material removal examined for molybdenum and copper CMP in weakly alkaline citrate-based slurries, Materials 17 (19) (2024) 4905, https://doi.org/10.3390/ma17194905.
[104] N. Schalk, Y. Moritz, G.K. Nayak, D. Holec, C. Hugenschmidt, V.V. Burwitz, L. Mathes, M. Schiester, C. Saringer, C. Czettl, M. Pohler, C. Mitterer, M. Tkadletz, Nanocomposite versus solid solution formation in the TiSiN system, Acta Mater. 275 (2024) 120063, https://doi.org/10.1016/j.actamat.2024.120063.
[105] C.-Y. Wang, C.-Y. Chou, H.-F. Shiue, H.-Y. Chen, C.-H. Ling, J.-J. Shyue, M.-J. Chen, Atomic layer annealing for modulation of the work function of TiN metal gate for n-Type MOS devices, Appl. Surf. Sci. 585 (2022) 152748, https://doi.org/10.1016/j.apsusc.2022.152748.
[106] H. Koerner, H.P. Erb, H. Melzner, Evaluation of Ti and TiN thicknesses for tungsten plug contact metallization, Appl. Surf. Sci. 73 (1993) 6–13, https://doi.org/10.1016/0169-4332(93)90139-3.
[107] S. Joseph, M. Eizenberg, C. Marcadal, L. Chen, TiSiN films produced by chemical vapor deposition as diffusion barriers for Cu metallization, J. Vac. Sci. Technol. B 20 (4) (2002) 1471–1476, https://doi.org/10.1116/1.1494068.
[108] S.H. Bae, S.-C. Song, K. Choi, G. Bersuker, et al., Thickness optimization of the TiN metal gate with polysilicon-capping layer on Hf-based high-k dielectric, Microelectronic Eng. 83 (3) (2006) 460–462, https://doi.org/10.1016/j.mee.2005.11.010.
[109] Y. Zeng, S.W. Russell, A.J. McKerrow, L. Chen, T.L. Alford, Effectiveness of Ti, TiN, Ta, TaN, and W_2N as barriers for the integration of low-k dielectric hydrogen silsesquioxane, J. Vac. Sci. Technol. B 18 (1) (2000) 221–228, https://doi.org/10.1116/1.591176.
[110] Q. Wan, H. Ding, M.I. Yousaf, Y.M. Chen, H.D. Liu, L. Hu, B. Yang, Corrosion behaviors of TiN and Ti-Si-N (with 2.9 at.% and 5.0 at.% Si) coatings by electrochemical impedance spectroscopy, Thin Solid Films 616 (2016) 601–607, https://doi.org/10.1016/j.tsf.2016.08.005.
[111] G. Greczynski, B. Bakhit, L. Hultman, M. Odén, High Si content TiSiN films with superior oxidation resistance, Surf. Coat. Technol. 398 (2020) 126087, https://doi.org/10.1016/j.surfcoat.2020.126087.
[112] S. Verhaverbeke, J.W. Parker, A model for the etching of Ti and TiN in SC-1 solutions, MRS Proc. 477 (1997) 447–452, https://doi.org/10.1557/PROC-477-447.
[113] G. Vereecke, H. De Coster, S. Van Alphen, P. Carolan, H. Bender, K. Willems, L.-Å. Ragnarsson, P. Van Dorpe, N. Horiguchi, F. Holsteyns, Wet etching of TiN in 1-D and 2-D confined nano-spaces of FinFET transistors, Microelectron. Eng. 200 (2018) 56–61, https://doi.org/10.1016/j.mee.2018.09.004.
[114] F. Piallat, R. Gassilloud, P. Caubet, C. Vallée, Investigation of TiN thin film oxidation depending on the substrate temperature at vacuum break, J. Vac. Sci. Technol. A 34 (5) (2016) 051508, https://doi.org/10.1116/1.4960648.
[115] H. Elmkhah, F. Attarzadeh, A. Fattah-alhosseini, K.H. Kim, Microstructural and electrochemical comparison between TiN coatings deposited through HIPIMS and DCMS techniques, J. Alloys Compd. 735 (2018) 422–429, https://doi.org/10.1016/j.jallcom.2017.11.162.
[116] C.-L. Chang, C.-T. Lin, P.-C. Tsai, W.-Y. Ho, W.-J. Liu, D.-Y. Wang, Mechanical and corrosion properties of (Ti,Si)N coating synthesized by cathodic arc plasma evaporation, Surf. Coat. Technol. 202 (22–23) (2008) 5516–5520, https://doi.org/10.1016/j.surfcoat.2008.06.029.
[117] K. Jun, Y. Shimogaki, Development of TiSiN CVD process using $TiCl_4/SiH_4/NH_3$ chemistry for ULSI anti-oxidation barrier applications, Sci. Technol. Adv. Mater. 5 (5–6) (2004) 549–554, https://doi.org/10.1016/j.stam.2004.03.002.
[118] E. Stevens, Y. Tomczak, B.T. Chan, E. Altamirano Sanchez, G.N. Parsons, A. Delabie, Area-Selective Atomic Layer deposition of TiN, TiO_2, and HfO_2 on silicon nitride with inhibition on amorphous carbon, Chem. Mater. 30 (10) (2018) 3223–3232, https://doi.org/10.1021/acs.chemmater.8b00017.
[119] T.-L. Liu, K.L. Nardi, N. Draeger, D.M. Hausmann, S.F. Bent, Effect of multilayer versus monolayer dodecanethiol on selectivity and pattern integrity in area-selective atomic layer deposition, ACS Appl. Mater. Interfaces 12 (37) (2020) 42226–42235, https://doi.org/10.1021/acsami.0c08873.
[120] M.J.M. Merkx, S. Vlaanderen, T. Faraz, M.A. Verheijen, W.M.M. Kessels, A.J. M. Mackus, Area-selective atomic layer deposition of TiN using aromatic inhibitor molecules for metal/dielectric selectivity, Chem. Mater. 32 (18) (2020) 7788–7795, https://doi.org/10.1021/acs.chemmater.0c02370.
[121] W.-J. Lee, E.-Y. Yun, H.-B.-R. Lee, S.W. Hong, S.-H. Kwon, Ultrathin effective TiN protective films prepared by plasma-enhanced atomic layer deposition for high-performance metallic bipolar plates of polymer electrolyte membrane fuel cells, Appl. Surf. Sci. 519 (2020) 146215, https://doi.org/10.1016/j.apsusc.2020.146215.
[122] N.D. Nam, D.S. Jo, J.G. Kim, D.H. Yoon, Corrosion protection of CrN/TiN multi-coating for bipolar plate of polymer electrolyte membrane fuel cell, Thin Solid Films 519 (20) (2011) 6787–6791, https://doi.org/10.1016/j.tsf.2011.01.207.
[123] M. Foucaud, D. Guiheux, D. Pinceau, P. Garnier, E. Pargon, R. Tiron, Investigation of the TiN/photoresist interface degradation during a wet etch, Microelectron. Eng. 135 (2015) 7–12, https://doi.org/10.1016/j.mee.2015.02.024.
[124] I. Ohkubo, Z. Hou, J.N. Lee, T. Aizawa, M. Lippmaa, T. Chikyow, K. Tsuda, T. Mori, Realization of closed-loop optimization of epitaxial titanium nitride thin-film growth via machine learning, Mater. Today Phys. 16 (2021) 100296, https://doi.org/10.1016/j.mtphys.2020.100296.
[125] K.V. Sagi, H.P. Amanapu, S.R. Alety, S.V. Babu, Potassium permanganate-based slurry to reduce the galvanic corrosion of the Cu/Ru/TiN Barrier liner stack during CMP in the BEOL interconnects, ECS J. Solid State Sci. Technol. 5 (5) (2016) P256–P263, https://doi.org/10.1149/2.0141605jss.
[126] R.P. Meethal, P. Jalalzai, K.S. Muskan, J. Peter, A. Klipp, T.-G. Kim, J.-G. Park, Benzethonium chloride as a tungsten corrosion inhibitor in neutral and alkaline media for the post-chemical mechanical planarization application, J. Colloid Interface Sci. 643 (2023) 465–479, https://doi.org/10.1016/j.jcis.2023.04.012.
[127] C. Li, D. Cai, D. Feng, Z. Cui, W. Liu, Z. Song, Chemical mechanical polishing of TiN film with potassium permanganate and L-aspartic acid in alkaline slurry, ECS J. Solid State Sci. Technol. 10 (7) (2021) 074009, https://doi.org/10.1149/2162-8777/ac164d.
[128] J. Jeong, A. Lee, J. Park, W. Jeon, Introducing Y_2O_3 passivation layer for utilizing TiSiN electrode on ZrO_2-based metal–insulator–metal capacitor applications, Appl. Surf. Sci. 679 (2025) 161267, https://doi.org/10.1016/j.apsusc.2024.161267.

[129] J. Ren, L. Xu, J. Luo, Z. Li, B. Li, X. Shi, L. Xu, L.T. Bang, Q. Fu, Hydrothermal oxidation of titanium nitride coating for enhanced corrosion resistance in fluoride-containing acidic solution, Mater. Lett. 335 (2023) 133790, https://doi.org/10.1016/j.matlet.2022.133790.
[130] X. Bai, L. Xu, X. Shi, J. Ren, L. Xu, Q. Wang, B. Li, Z. Liu, C. Zheng, Q. Fu, Hydrothermal oxidation improves corrosion and wear properties of multi-arc ion plated titanium nitride coating for biological application, Vacuum 198 (2022) 110871, https://doi.org/10.1016/j.vacuum.2022.110871.
[131] X. Shi, L. Xu, T.B. Le, G. Zhou, C. Zheng, K. Tsuru, K. Ishikawa, Partial oxidation of TiN coating by hydrothermal and ozone (O_3) treatment in pure water, Mater. Sci. Eng. C 59 (2016) 542–548, https://doi.org/10.1016/j.msec.2015.10.024.
[132] R. Hao, W. Miao, W. Xu, Y. Lin, Q. Xiao, Z. Wang, Q. Li, P. Wang, T. Wang, A. Nie, J. Wu, H. Wang, Unraveling the atomic structure evolution of titanium nitride upon oxidation, Corros. Sci. 240 (2024) 112465, https://doi.org/10.1016/j.corsci.2024.112465.
[133] I. Martinez, B. Matijević, In situ electrochemical impedance spectroscopy of TiN-based hard coatings, J. Electrochem. Sci. Eng. 15 (4) (2025) 2709, https://doi.org/10.5599/jese.2709.
[134] Y. Cheng, S. Wang, C. Wang, D. Yang, Glycine as an efficient corrosion inhibitor for TiN oxidation environments, ECS J. Solid State Sci. Technol. 12 (2) (2023) 023012, https://doi.org/10.1149/2162-8777/acbbe8.
[135] L. Broussous, S. Zoll, H. Ishikawa, F. Buisine, A. Lamaury, Contact cleaning opportunities on single wafer tool, Microelectron. Eng. 192 (2018) 8–13, https://doi.org/10.1016/j.mee.2018.01.016.
[136] S.Y. Lee, J. Mack, H.Y. Kim, S.-H. Jung, S.J. Rathi, N. Mukherjee, Diffusion barrier properties of atomic layer deposited TiSiN films, Mater. Lett. 315 (2022) 131912, https://doi.org/10.1016/j.matlet.2022.131912.
[137] R. Akhter, Z. Zhou, Z. Xie, P. Munroe, TiN versus TiSiN coatings in indentation, scratch and wear setting, Appl. Surf. Sci. 563 (2021) 150356, https://doi.org/10.1016/j.apsusc.2021.150356.
[138] P.B. Zantye, A. Kumar, A.K. Sikder, Chemical mechanical planarization for microelectronics applications, Mater. Sci. Eng. R. Rep. 45 (3–6) (2004) 89–220, https://doi.org/10.1016/j.mser.2004.06.002.
[139] Y. Cui, J.Y. Jeong, Y. Gao, S.G. Pyo, Effect of contact plug deposition conditions on junction leakage and contact resistance in multilevel CMOS logic interconnection device, Micromachines 11 (2) (2020) 170, https://doi.org/10.3390/mi11020170.
[140] A. Goda, Recent progress on 3D NAND flash technologies, Electronics 10 (24) (2021) 3156, https://doi.org/10.3390/electronics10243156.
[141] S. Marschmeyer, J. Berthold, A. Krüger, M. Lisker, A. Scheit, S. Schulze, A. Trusch, M. Wietstruck, D. Wolansky, Modular integration of annular TSV structures filled with tungsten in a 0.25 μm SiGe:C BiCMOS technology, Microelectron. Eng. 137 (2015) 153–157, https://doi.org/10.1016/j.mee.2014.09.020.
[142] Y. Tsuji, M. Terai, S. Fujieda, T. Syo, T. Saito, K. Ando, A novel method for evaluating electron/hole mismatch in scaled split-gate SONOS memories, IEEE Trans. Electron Devices 48 (12) (2001) 2634–2640, https://doi.org/10.1109/IEDM.2008.4796691.
[143] S. Bothra, H. Sur, V. Liang, A new failure mechanism by corrosion of tungsten in a tungsten plug process, Microelectron. Reliab. 39 (1) (1999) 59–68, https://doi.org/10.1016/S0026-2714(98)00191-7.
[144] H. Chen, R. Fan, H. Lou, Y. Huang, Electrochemical mechanism of layout-dependent corrosion of tungsten in contact plugs, Mater. Sci. Semicond. Process. 20 (2014) 17–22, https://doi.org/10.1016/j.mssp.2013.12.029.
[145] J. Seo, K. You, J. Moon, J.H. Kim, U. Paik, Corrosion behavior of tungsten metal gate in the presence of hydrogen peroxide at acidic medium, ECS J. Solid State Sci. Technol. 6 (4) (2017) P169–P171, https://doi.org/10.1149/2.0311704jss.
[146] T. Parson, S.-N. Jenq, S. Medd, D. White, M. White, D. Frye, Tungsten post-CMP cleaning composition. U.S. Patent 10,988,718 B2, Apr 27, 2021.
[147] Y. Yao, B. Pan, W. Wang, S. Tan, Effects of benzotriazole and imidazoline on the tribocorrosion behaviors of a WC-based material in saline silica slurries, Int. J. Refract. Met. Hard Mater 97 (2021) 105523, https://doi.org/10.1016/j.ijrmhm.2021.105523.
[148] K. Lee, J. Seo, Suppression of dissolution rate via coordination complex in tungsten chemical mechanical planarization, Appl. Sci. 12 (3) (2022) 1227, https://doi.org/10.3390/app12031227.
[149] R.P. Meethal, S. Kumar, M. Yadav, P. Jalalzai, A. Klipp, T.-G. Kim, J.-G. Park, Polyethyleneimine polymer as an effective corrosion inhibitor for advanced node tungsten post-CMP cleaning, Appl. Surf. Sci. 716 (2026) 164670, https://doi.org/10.1016/j.apsusc.2025.164670.
[150] D. Pan, G. Ren, J. Zhang, L. Wang, S. Wang, Study on amino acid corrosion inhibitors in tungsten chemical mechanical planarization, ECS J. Solid State Sci. Technol. 13 (12) (2024) 124004, https://doi.org/10.1149/2162-8777/ad9a7c.
[151] N. Jia, C. Wang, C. Zhang, J. Liu, Effect of tannic acid on the corrosion behavior of W18Cr4V in a simulated wood environment and its inhibition mechanism, Forests 14 (2023) 1781, https://doi.org/10.3390/f14091781.
[152] N.A. Shapagina, V.V. Dushik, Application of electrophoretic deposition as an advanced technique of inhibited polymer films formation on metals from environmentally safe aqueous solutions of inhibited formulations, Materials 16 (1) (2023) 19, https://doi.org/10.3390/ma16010019.
[153] N.A. Shapagina, A.V. Shapagin, V.V. Dushik, A.A. Shaporenkov, U.V. Nikulova, V. Y. Stepanenko, V.V. Matveev, A.L. Klyuev, B.A. Loginov, Methods of formation of protective inhibited polymer films on tungsten, Int. J. Mol. Sci. 24 (19) (2023) 14412, https://doi.org/10.3390/ijms241914412.
[154] S. Lee, C.-J. Ni, A study of the effect of post-metal etch wet cleaning processes and silicon oxynitride film on charge induced corrosion of tungsten vias, Mater. Sci. Semicond. Process. 13 (5–6) (2011) 315–319, https://doi.org/10.1016/j.mssp.2011.02.011.
[155] E.A. Kuzina, K.A. Emelyanenko, M.A. Teplonogova, A.M. Emelyanenko, L. B. Boinovich, Durable superhydrophobic coatings on tungsten surface by nanosecond laser ablation and fluorooxysilane modification, Materials 16 (1) (2023) 196, https://doi.org/10.3390/ma16010196.
[156] F.H. Li, J.D. Fabbri, R.I. Yurchenko, A.N. Mileshkin, J.N. Hohman, H. Yan, H. Yuan, I.C. Tran, T.M. Willey, M. Bagge-Hansen, J.E.P. Dahl, R.M.K. Carlson, A. A. Fokin, P.R. Schreiner, Z.-X. Shen, N.A. Melosh, Covalent attachment of diamondoid phosphonic acid dichlorides to tungsten oxide surfaces, Langmuir 29 (30) (2013) 9790–9797, https://doi.org/10.1021/la401781e.
[157] M. Anik, T. Cansizoglu, Dissolution kinetics of WO_3 in acidic solutions, J. Appl. Electrochem. 36 (2006) 603–608, https://doi.org/10.1007/s10800-006-9113-3.
[158] A. Pacco, T. Nakano, J. Loyo Prado, J.-G. Lai, H. Kawarazaki, E. Altamirano Sanchez, Etching of tungsten via a combination of thermal oxide formation and wet-chemical oxide dissolution, Microelectron. Eng. 297 (2024) 112304, https://doi.org/10.1016/j.mee.2024.112304.
[159] J. Knöppel, A. Kormányos, B. Mayerhöfer, A. Hofer, M. Bierling, J. Bachmann, S. Thiele, S. Cherevko, Photocorrosion of WO_3 photoanodes in different electrolytes, ACS Phys. Chem. Au 1 (1) (2021) 6–13, https://doi.org/10.1021/acsphyschemau.1c00004.
[160] M. Togaru, R. Sainju, L. Zhang, W. Jiang, Y. Zhu, Direct observation of tungsten oxidation studied by in situ environmental TEM, Mater Charact 174 (2021) 111016, https://doi.org/10.1016/j.matchar.2021.111016.
[161] J.-H. Lim, J.-H. Park, J.-G. Park, Effect of iron(III) nitrate concentration on tungsten chemical-mechanical-planarization performance, Appl. Surf. Sci. 282 (2013) 512–517, https://doi.org/10.1016/j.apsusc.2013.06.003.
[162] M.K. Poddar, P. Jalalzai, S. Sahir, N.P. Yerriboin, T.-G. Kim, J.-G. Park, Tungsten passivation layer (WO_3) formation mechanisms during chemical mechanical planarization in the presence of oxidizers, Appl. Surf. Sci. 537 (2021) 147862, https://doi.org/10.1016/j.apsusc.2020.147862.
[163] L. Xu, L. Wang, H. Chen, X. Wang, F. Chen, B. Lyu, W. Hang, W. Zhao, J. Yuan, Effects of pH values and H_2O_2 concentrations on the chemical enhanced shear dilatancy polishing of tungsten, Micromachines 13 (5) (2022) 762, https://doi.org/10.3390/mi13050762.
[164] J.T. Lee, S. Hati, M.M. Fahey, J.M. Zaleski, R. Sardar, Surface-ligand-controlled enhancement of carrier density in plasmonic tungsten oxide nanocrystals: spectroscopic observation of trap-state passivation via multidentate metal phosphonate bonding, Chem. Mater. 34 (2022) 3053–3066, https://doi.org/10.1021/acs.chemmater.1c04042.
[165] Z. Zhang, H. Mo, R. Li, X. Zhou, Z. Lin, J. Zhang, X. Tang, Y. Zhan, J. Luo, The counterbalancing role of oxygen vacancy between the electrochromic properties and the trapping effect passivation for amorphous tungsten oxide films, Small Sci. 4 (2024) 2300219, https://doi.org/10.1002/smsc.202300219.
[166] L. Wang, F. Peng, H. Chen, W. Hang, C. Yu, S. Chen, S. Zhao, Z. Wu, Y. Ma, B. Lyu, J. Yuan, The influence of pH and H_2O_2 on surface quality and material removal rate during W-CMP, Int. J. Adv. Manuf. Technol. 127 (2023) 4097–4110, https://doi.org/10.1007/s00170-023-11805-3.
[167] V.M. Volgin, T.B. Kabanova, A.D. Davydov, Theoretical analysis of mass transfer during anodic dissolution of tungsten rotating disk electrode in alkaline solutions, Electrochim. Acta 336 (2020) 135705, https://doi.org/10.1016/j.electacta.2020.135705.
[168] V. Suman, R.S. Maurya, T. Laha, D. Chaira, Exceptional low-temperature fabrication of self-passivating tungsten alloys by mechanical alloying and spark plasma sintering, J. Mater. Eng. Perform. 34 (14) (2025) 14110–14125, https://doi.org/10.1007/s11665-024-10212-3.
[169] R.R. Lieten, D. White, T. Parson, S. Jenq, D. Frye, M. White, L. Teugels, H. Struyf, Post-CMP cleaners for tungsten advanced nodes: 10 nm and 7 nm. In Proc. Int. Conf. Planarization/CMP Technol. (ICPT 2017); Leuven, Belgium, Oct 11–13, 2017; pp 155–160.
[170] D. White, T. Parson, S. Jenq, D. Frye, S. Medd, R. Lietenc, M. White, L. Teugels, Post-CMP cleaners for tungsten at advanced nodes, Solid State Phenom. 255 (2016) 186–191, https://doi.org/10.4028/www.scientific.net/SSP.255.186.
[171] W.-T. Tseng, P. Chu, S. Siddiqui, D. Canaperi, Y.-P. Huang, K. Gramigna, P. Hsu, P. Bernatis, Post tungsten CMP cleaning: optimization for cleaning efficiency and corrosion reduction, ECS J. Solid State Sci. Technol. 13 (11) (2024) 114004, https://doi.org/10.1149/2162-8777/ad8f61.
[172] S. Ma, Y. Du, S. Wang, Y. Su, Application of machine learning in material corrosion research, Corros. Rev. 41 (4) (2023) 417–426, https://doi.org/10.1515/corrrev-2022-0089.
[173] A. Fateh, M. Aliofkhazraei, A.R. Rezvanian, Review of corrosive environments for copper and its corrosion inhibitors, Arab. J. Chem. 13 (1) (2020) 481–544, https://doi.org/10.1016/j.arabjc.2017.05.021.
[174] M.M. Antonijevic, M.B. Petrovic, Copper corrosion inhibitors. A review, Int. J. Electrochem. Sci. 3 (2008) 1–28.
[175] M. Metikos-Hukovic, R. Babic, I. Paic, Copper corrosion at various pH values with and without the inhibitor, J. Appl. Electrochem. 30 (2000) 617–624, https://doi.org/10.1023/A:1003956102631.
[176] J.J. Shim, J.G. Kim, Copper corrosion in potable water distribution systems: influence of copper products on the corrosion behavior, Mater. Lett. 58 (17–18) (2004) 2002–2006, https://doi.org/10.1016/j.matlet.2003.12.017.
[177] X. She, J. Peng, Y. Qiang, Y. Zhou, S. Zhang, Recent advances in protective technologies against copper corrosion, J. Mater. Sci. Technol. 201 (2024) 75–94, https://doi.org/10.1016/j.jmst.2024.02.060.

[178] M. Lasri, A. Ait-karra, O. Zakir, R. Idouhli, B. Dikici, M.E. Khadiri, A. Abouelfida, Copper corrosion in chloride environments: key inhibitors and strategies, J. Bio Tribo-Corros. 11 (2025) 60, https://doi.org/10.1007/s40735-025-00980-3.
[179] Y.H. Lei, N. Sheng, A. Hyono, M. Ueda, T. Ohtsuka, Effect of benzotriazole (BTA) addition on polypyrrole film formation on copper and its corrosion protection, Prog. Org. Coat. 77 (2014) 339–346, https://doi.org/10.1016/j.porgcoat.2013.10.009.
[180] S. Wan, C.-H. Miao, R.-M. Wang, Z.-F. Zhang, Z.-H. Dong, Enhanced corrosion resistance of copper by synergetic effects of silica and BTA codoped in polypyrrole film, Prog. Org. Coat. 129 (2019) 187–198, https://doi.org/10.1016/j.porgcoat.2019.01.014.
[181] M. Friedrich, J.C. Gálvez-Ruiz, T.M. Klapötke, P. Mayer, B. Weber, J.J. Weigand, BTA copper complexes, Inorg. Chem. 44 (22) (2005) 8044–8052, https://doi.org/10.1021/ic050657r.
[182] J. Gao, Q. Wang, L. Dong, J. Ren, X. Chai, K. Song, Construction and corrosion resistance mechanism of BTA passivation film on B30 cupronickel, Surf. Coat. Technol. 515 (2025) 132585, https://doi.org/10.1016/j.surfcoat.2025.132585.
[183] C. Cao, X. Li, Y. Chen, J. Liu, Understanding N-site substituents effect on corrosion inhibition performance of benzotriazole derivatives in copper chemical mechanical planarization: theoretical and experimental analysis, Mater. Today Chem. 47 (2025) 102850, https://doi.org/10.1016/j.mtchem.2025.102850.
[184] X. Cheng, C. Guo, L. Lu, L. Pan, Evaluation for the synergistic corrosion inhibition properties of benzotriazole and decanoic acid compound formulation volatile corrosion inhibitors, Mater. Today Commun. 48 (2025) 113526, https://doi.org/10.1016/j.mtcomm.2025.113526.
[185] M. Lasri, M. Fawzi, O. Zakir, A. Hasnaoui, R. Idouhli, M. Maatallah, K. Mohyeddine, M.Y. Ait Itto, A. Auhmani, A. Abouelfida, Exploring the effectiveness of two triazole derivatives as copper corrosion inhibitors in NaCl solution: a combined approach of quantitative chemistry and dynamic molecular simulations, J. Mol. Struct. 1303 (2024) 137593, https://doi.org/10.1016/j.molstruc.2024.137593.
[186] P.P. Samal, C.P. Singh, S. Tiwari, V. Shah, S. Krishnamurty, Indazole-5-amine (AIA) as competing corrosion coating to benzotriazole (BTAH) at the interface of Cu: a DFT and BOMD case study, Comput. Theor. Chem. 1239 (2024) 114762, https://doi.org/10.1016/j.comptc.2024.114762.
[187] L. Dai, Z. Yan, Y. Wang, D. Zhang, Novel tetrazole inhibitors for alkaline Cu-CMP: experimental and theoretical studies, Surf. Interfaces 72 (2025) 106947, https://doi.org/10.1016/j.surfin.2025.106947.
[188] L. Hu, Q. Chen, J. He, W. Sun, J. Huang, Y. Zhang, G. Pan, Y. Xu, Experimental and computational investigation of salicylhydroxamic acid as a corrosion inhibitor for copper in alkaline solutions, ECS J. Solid State Sci. Technol. 13 (9) (2024) 094002, https://doi.org/10.1149/2162-8777/ad7b76.
[189] S.A. Mahdy, S.A. Abdel-Gawad, R.M. El-Sherif, I.M. Ghayad, Comparative studies of tetrazole derivatives on the corrosion inhibition of copper and commercial brass in simulated seawater, Discover Appl. Sci. 6 (2024) 136, https://doi.org/10.1007/s42452-024-05778-5.
[190] C. Cao, X. Li, Y. Chen, J. Liu, S. Wu, X. Shen, Y. Dai, M. Wang, D. Tong, C. Shi, F. Meng, J. Feng, J. Ni, Near-atomic surfaces of copper achieved with eco-friendly humus as an alternative corrosion inhibitor in sustainable chemical mechanical planarization, Langmuir 41 (27) (2025) 17679–17691, https://doi.org/10.1021/acs.langmuir.5c01316.
[191] T.T.H. Tran, J. Gichovi, J. Commane, E.J. Podlaha, J. Seo, Examining amino acids as environmentally friendly corrosion inhibitors for Cu and Co chemical mechanical planarization, J. Environ. Chem. Eng. 12 (2024) 113669, https://doi.org/10.1016/j.jece.2024.113669.
[192] J. Seo, S. Ryu, J. Kwon, K. Lee, Structural dependency of pyridine carboxylic acid isomers in metal-organic coordination adsorption for copper corrosion inhibition, Appl. Surf. Sci. 663 (2024) 160149, https://doi.org/10.1016/j.apsusc.2024.160149.
[193] X. Wang, W. Li, B. Tan, F. Wang, H. Du, R. Liu, X. Han, S. Zhang, Corrosion inhibition effect of benzimidazole and two derivatives on copper in alkaline environments: experimental and theoretical analyses, J. Mol. Liq. 390 (2023) 122985, https://doi.org/10.1016/j.molliq.2023.122985.
[194] X. Yu, Z. Xue, H. Chen, W. Li, H. Li, J. Hu, J. Zhang, Q. Chen, G. Hou, Y. Tang, Research on chromium-free passivation and corrosion performance of pure copper, Materials 18 (19) (2025) 4585, https://doi.org/10.3390/ma18194585.
[195] Y.I. Kuznetsov, G.V. Redkina, Thin protective coatings on metals formed by organic corrosion inhibitors in neutral media, Coatings 12 (2) (2022) 149, https://doi.org/10.3390/coatings12020149.
[196] K.W. Shinato, A.A. Zewde, Y. Jin, Corrosion protection of copper and copper alloys in different corrosive medium using environmentally friendly corrosion inhibitors, Corros. Rev. 38 (2) (2020) 101–109, https://doi.org/10.1515/corrrev-2019-0105.
[197] J. Muhammad Yelwa, H. Musa, O.O. Fasanya, J. Yusuf Yahaya, Corrosion-resistant coatings: advances in deposition methods, nanostructures, and self-healing films, Acad. Mater. Sci. 2 (2025) 1–30, https://doi.org/10.20935/AcadMatSci7829.
[198] A. Thakur, S. Kaya, A. Kumar, Recent trends in the characterization and application progress of nano-modified coatings in corrosion mitigation of metals and alloys, Appl. Sci. 13 (2023) 730, https://doi.org/10.3390/app13020730.
[199] F.-S. Razavi, M. Shabani-Nooshabadi, M. Behpour, Sol-Gel synthesis, characterization and electrochemical corrosion behavior of S-N-C-Doped TiO_2 nano coating on copper, J. Mol. Liq. 266 (2018) 99–105, https://doi.org/10.1016/j.molliq.2018.06.056.
[200] A. Rajput, A. Mishra, S. Atal, F.S. Gill, S. Juyal, G. Bansal, Barrier coating of superhydrophobically modified nano zirconia on copper: study of electrochemical anti-corrosion properties, Anti-Corros. Methods Mater. 72 (4) (2025) 533–547, https://doi.org/10.1108/ACMM-08-2024-3065.
[201] E. Pezić, N. Matijaković Mlinarić, J. Kovač, P. Dubček, D. Kralj, K. Marušić, Optimizing the preparation of polymer nanocoatings by self-assembly and gamma irradiation of elaidic acid on copper surfaces, Prog. Org. Coat. 192 (2024) 108514, https://doi.org/10.1016/j.porgcoat.2024.108514.
[202] Y. Zhang, B. Tan, X. Zhang, L. Guo, S. Zhang, Synthesized carbon dots with high N and S content as excellent corrosion inhibitors for copper in sulfuric acid solution, J. Mol. Liq. 338 (2021) 116702, https://doi.org/10.1016/j.molliq.2021.116702.
[203] X. Gao, Y. Gao, H. Cao, J. Zhang, Eco-friendly sustainable and responsive high-performance benzotriazole–metal organic frameworks/silica composite coating with active/passive corrosion protection on copper, Langmuir 40 (14) (2024) 7639–7652, https://doi.org/10.1021/acs.langmuir.4c00328.
[204] H. Zhang, H. Bian, X. Zhang, L. Zhang, Y. Chen, Y. Yang, Z. Zhang, Preparation and characterization of hollow ceria-based smart anti-corrosive coatings on copper, Surf. Interfaces 45 (2024) 103930, https://doi.org/10.1016/j.surfin.2024.103930.
[205] R. Mahesh, A. Jain, Y.C.S. Kumar, A.V. Raghu, Plant extracts and green nanocomposites as sustainable corrosion inhibitors: a comprehensive review, Sustain. Chem. One World 8 (2025) 100132, https://doi.org/10.1016/j.scowo.2025.100132.
[206] M. Gabsi, H. Ferkous, A. Delimi, A. Boublia, C. Boulechfar, A. Kahlouche, A. S. Darwish, T. Lemaoui, Y. Benguerba, The curious case of polyphenols as green corrosion inhibitors: a review on their extraction, design, and applications, Environ. Sci. Pollut. Res. 30 (2023) 59081–59105, https://doi.org/10.1007/s11356-023-26753-4.
[207] S. Bilgiç, Plant extracts as corrosion inhibitors against copper corrosion – an overview, Int. J. Corros. Scale Inhib. 12 (3) (2023), https://doi.org/10.17675/2305-6894-2023-12-3-24.
[208] M. Rađošić, N.D. Nikolić, A. Salicio-Paz, E. García-Lecina, L.S. Živković, J.B. Bajat, Zn-Co-CeO2 vs. Zn-Co coatings: effect of CeO2 sol in the enhancement of the corrosion performance of electrodeposited composite coatings, Metals 11 (5) (2021) 704, https://doi.org/10.3390/met11050704.
[209] S. Al Zerey, Impact of interconnect scaling on copper microstructure and electromigration reliability in copper/dielectric hybrid bonding, Binghamton University, State University of New York, Binghamton, NY, 2025. Ph.D. Dissertation.
[210] H. Du, F. Wang, X. Wang, B. Tan, Y. Shi, R. Liu, X. Han, Synergistic effect of composite complex agent on BTA removal in post-Cu-CMP: experimental and theoretical analysis, ECS J. Solid State Sci. Technol. 12 (12) (2023) 124003, https://doi.org/10.1149/2162-8777/ad1616.
[211] J. Zhao, F. Wang, Y. Xu, B. Tan, X. Zhao, S. Zhang, X. Han, R. Liu, Corrosion inhibitors in H2O2 system slurry for Ru based barrier layer cu interconnect chemical mechanical polishing and optimization, Colloids Surf A Physicochem Eng Asp (2024) 135351, https://doi.org/10.1016/j.colsurfa.2024.135351.
[212] K. Gamagedara, D. Roy, Experimental strategies for studying tribo-electrochemical aspects of chemical–mechanical planarization, Lubricants 12 (2) (2024) 63, https://doi.org/10.3390/lubricants12020063.
[213] S. Wang, T. Liu, F. Dong, Y. Sun, L. Xue, R. Li, X. Han, Z. Tian, S. Liu, Surface action mechanism and design considerations for the mechanical integrity of Cu/low K BEOL interconnect during chemical mechanical polishing process, Microelectron. Reliab. 134 (2022) 114565, https://doi.org/10.1016/j.microrel.2022.114565.